Research Updates

Exploration of complex nanostructures in block copolymers

Hojun Lee, Jihoon Kim, and Moon Jeong Park*
Department of Chemistry, Pohang University of Science and Technology (POSTECH), Pohang, Gyeongsangbuk-do 37673, Republic of Korea

(Received 20 November 2023; accepted 16 January 2024; published 13 February 2024)

The exploration of nanoscale morphologies with three-dimensional spatial arrangements in block copolymers involves the manipulation of compositional fluctuations at interfaces, induction of conformational asymmetry, and design of complex architectures. Despite the abundance of triply periodic minimal surfaces identified to date, the experimental demonstration of thermodynamically stable complex nanostructures with high-packing frustration remains limited. This research update focuses on the importance of molecular interactions for stabilizing complex nanostructures and proposes the use of end-group chemistry as a versatile method for realizing thermodynamically stable network structures with high-packing frustration in simple linear diblock copolymers. The proposed approach substantially alters phase diagrams and reveals unprecedented network structures in block copolymers. Ongoing research has the potential to generate even more diverse and stable nanostructures, thereby advancing nanotechnology and expanding our understanding of polymers and materials science.

DOI: 10.1103/PhysRevMaterials.8.020302

I. INTRODUCTION

Materials science has experienced remarkable evolution due to the unceasing pursuit of materials transcending conventional boundaries and exhibiting meticulously tailored properties and functionalities [1,2]. Among such materials, which have been carefully evaluated in terms of their utility for tackling modern technological hurdles and scientific goals [3,4], block copolymers have emerged as versatile building blocks for nanostructure design and fabrication [5–7].

Block copolymers are composed of two or more chemically dissimilar polymer chains and consequently exhibit microphase separation. This allows their spontaneous organization into nanoscale domains ranging from simple lamellar, cylindrical, and spherical structures to more complex bicontinuous phases, depending on the delicate balance between the interfacial tension and stretching energy of the polymer chains [8,9]. The pioneering works of Helfand in 1975 [10,11] and Leibler in 1980 [12] established the key parameters governing this equilibrium, including the block volume fraction (f), degree of polymerization (N), and Flory-Huggins interaction parameter (χ).

The precise control over the size and shape of the above-mentioned domains enables the manipulation of material properties at the nanoscale [13]. In particular, considerable attention has been directed towards block copolymers that exhibit nanoscale morphologies with three-dimensional (3D) spatial arrangements owing to their potential applications in catalysis [14], sensing [15], photonic devices [16], and advanced display technologies [17,18] due to their inherently high surface-area-to-volume ratios [19,20] and unique optical characteristics [21,22]. Furthermore, the exploration of complex phases has advanced scientific knowledge, e.g., the recent discovery of topologically close-packed phases, known as Frank-Kasper (FK) phases, in block copolymers has opened a new forum in polymer science [23].

The 3D self-assembly of block copolymers can afford complex network morphologies with interconnected channel structures suitable for highly efficient charge transport/storage [24,25] and, hence, the development of high-performance energy storage and conversion devices. The gyroid was the first network structure observed in weakly segregated block copolymers [26] and later theoretically proven to be stable in the high χN region [27]. However, gyroid structures exist within narrow phase diagram regions and therefore have limited practical applications, which highlights the importance of understanding the thermodynamics and kinetics of the 3D self-assembly of block copolymers.

Continued experimental [28] and theoretical [29,30] investigations aiming to uncover the various network structures in block copolymers are crucial because some of these complex structures are regarded as thermodynamically unstable for soft materials [31] and their discovery is more commonly associated with inorganic compounds [32,33]. Hence, researchers need to determine the mechanisms of network structure development in block copolymers and the key factors affecting the stability of these structures. Currently, high-packing-frustration morphologies formed by block copolymers are scarce, and the mechanisms for stabilizing such polymorphs

*Corresponding author: moonpark@postech.ac.kr

with controlled intermolecular interactions remain largely unexplored.

This research update deals with the self-assembly of block copolymers and its underlying principles, examining the resulting intricate network morphologies from the viewpoints of thermodynamics and kinetics and highlighting the recent advances in their design to illuminate the future of polymer science and nanotechnology.

II. CONSTRUCTION OF TRIPLY PERIODIC MINIMAL SURFACES IN BLOCK COPOLYMERS

A. Strategies for stabilizing gyroid structures

Triply periodic minimal surfaces observed in block copolymers typically exhibit cubic symmetry. Examples of such surfaces include the gyroid (G), diamond (D), and primitive (P). The G surface exhibits a framework consisting of three tubes extending from a single node (threefold), characterized by a singular network ($I4_132$) and interwoven double networks ($Ia\bar{3}\ d$). On the other hand, the D surface possesses a network with tetrahedral connectivity (fourfold), with distinct symmetries based on whether it is a single ($Fd\bar{3}\ m$) or double ($Pn\bar{3}\ m$) network. The P surface is less common and has a six-coordinate interconnected network (sixfold), distinguishable by single ($Pm\bar{3}\ m$) and double ($Im\bar{3}\ m$) networks. Triply periodic equilibrium structures, diverging from cubic symmetry, have also been observed in block copolymers. These structures include the orthorhombic network (O^{70}) with the *Fddd* space group. In Fig. 1(a), the gyroid, diamond, primitive, and orthorhombic network structures are illustrated.

The primary challenge of obtaining triply periodic minimal surfaces in block copolymers is their inherent topological complexity [34]. Self-consistent field theory (SCFT) calculations revealed that cylinder structures minimize interfacial area with nearly constant mean curvature interface. On the other hand, gyroid intersections exhibit considerable curvature variations [Fig. 1(b)] [35]. This behavior is even more pronounced for perforated structures, resulting in substantial deviations in the mean curvature. Such variations disrupt chain packing and make these structures difficult to access experimentally.

The manipulation of the microphase separation behavior of block copolymers has mainly involved fine-tuning the balance between interfacial tension and stretching energy. In this context, several approaches have been developed to increase the stability of gyroid structures without excessive chain stretching and alleviate packing frustration, as exemplified by the synthesis of tapered diblock copolymers via the modification of the interfacial chemical composition [Fig. 1(c)] [36]. Epps and co-workers designed a set of tapered copolymers using polystyrene-*b*-polyisoprene block copolymers, in which the sharp interface between the two blocks was transformed into a gradient region with gradual composition changes [36]. The length of the tapered region can be adjusted to modify the stability window of gyroid structures, as theoretically substantiated by Hall and co-workers [37]. The expanded gyroid region observed in tapered copolymers was explained by an increased interfacial width, which lowers the expenditure of free energy near the interfaces to alleviate packing frustration in tripod intersections.

Segalman and co-workers tuned the phase window of gyroid structures in polystyrene-*b*-polypeptoid (PS-*b*-PEP) block copolymers by incorporating small junctions with two different conformations [38]. Figure 1(d) shows that this window is much broader for a coil-shaped junction than for a helical-shaped junction, which is attributed to the greater space-filling capacity of the flexible interfacial segment (coil) compared to that of the more rigid and compact junction (helix) at the interface.

Another method for alleviating packing frustration in diblock copolymers involves polydispersity index (PDI) modification, e.g., higher PDIs increase the stability of gyroid structures because longer chains can effectively fill the thicker core of the tripod intersections therein [Fig. 1(e)] [39–41]. Alternatively, diblock copolymers can be blended with homopolymers of the same chemical composition as minor blocks to improve the space-filling capability within the bulky core of the channel structures. This selective homopolymer localization is related to the lower free energy of the node [42–44].

B. Complex network structures beyond gyroid

The realm of intricate complex network structures formed in block copolymers can be expanded by developing linear multiblock copolymers [45]. ABC triblock copolymers were employed as model systems, and their phase behavior was predicted and controlled using principles similar to those used for AB diblock copolymers. The complex morphologies of ABC triblock copolymers arise from the need to minimize stretching and interfacial energy across three distinct domains and are therefore strongly influenced by block arrangement. Intriguingly, ABC triblock copolymers offer a broad spectrum of network structures beyond double gyroid (DG) formation.

Figure 2 presents the diverse 3D network morphologies observed in ABC triblock copolymer systems [45]. Matsushita *et al.* studied polyisoprene-*b*-polystyrene-*b*-poly(2-vinylpyridine) (PI-*b*-PS-*b*-P2VP) triblock copolymers and observed tricontinuous gyroid structures ($I4_132$) when the volume fraction of the PS block fell within the range that stabilizes hexagonal (hex) and lamellae (lam) structures in diblock architecture [46]. Bates and co-workers revealed that a core-shell gyroid structure was formed in polyisoprene-*b*-polystyrene-*b*-poly(dimethyl siloxane) (PI-*b*-PS-*b*-PDMS) triblock copolymers when the volume fractions of the PS and PI blocks were comparable, with PDMS constituting a smaller fraction [47]. In this structure, PDMS domains formed two intertwined threefold networks enclosed by PS shells, whereas PI blocks occupied the remaining space, which resulted in the formation of five distinct domains continuous in all three dimensions.

Bates and co-workers further explored polyisoprene-*b*-polystyrene-*b*-poly(ethylene oxide) (PI-*b*-PS-*b*-PEO) triblock copolymers of various compositions and discovered the first noncubic triply periodic network morphology, the orthorhombic network (*Fddd*), in block copolymer systems [48]. Subsequently, Hasegawa and co-workers observed the *Fddd* phase in PS-*b*-PI diblock copolymers, although its

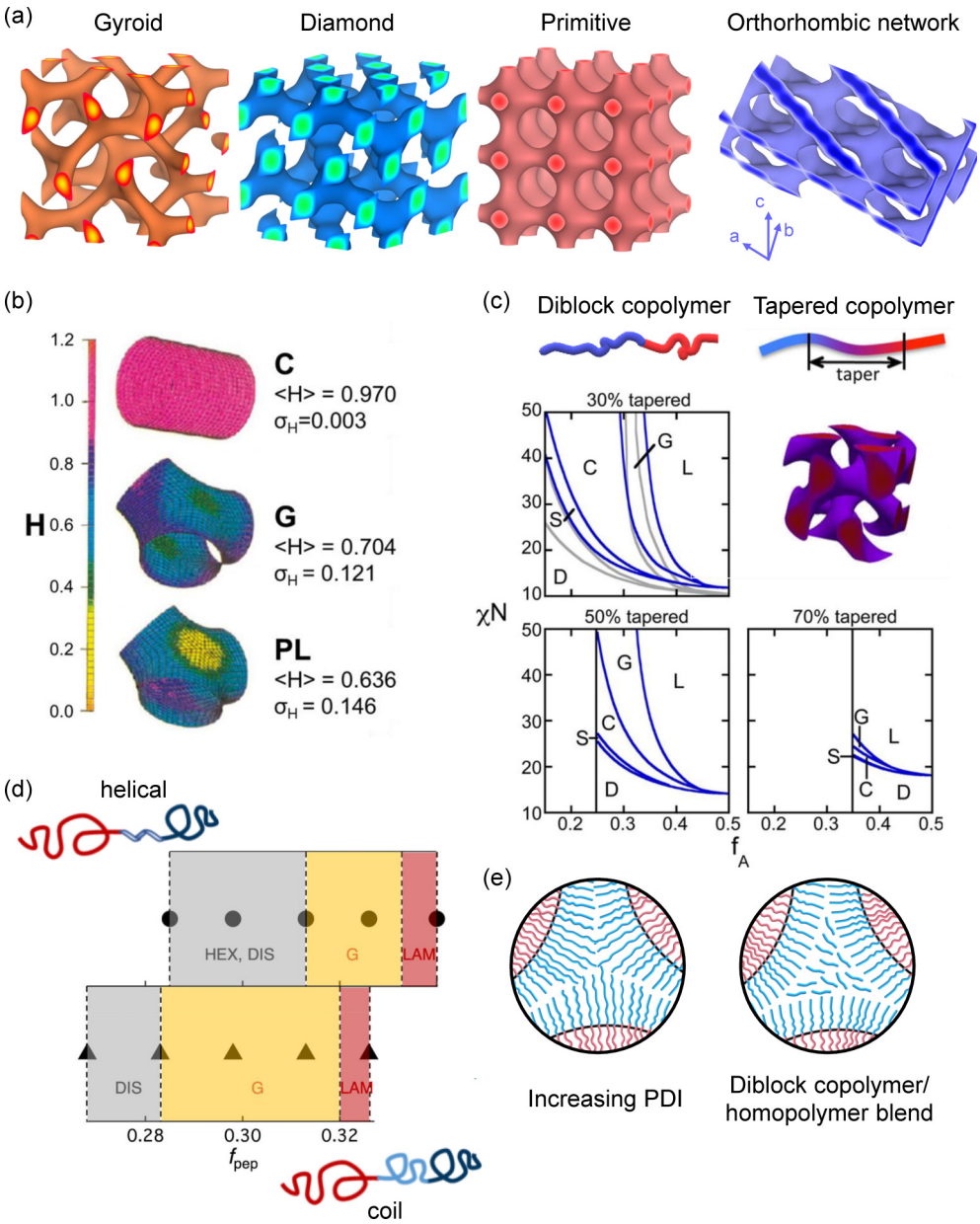

FIG. 1. (a) Representative triply periodic structures (gyroid, diamond, primitive, and orthorhombic network) observed in block copolymers. (b) Self-consistent field theory (SCFT) -calculated interfacial surfaces associated with elementary units of cylinder (C), gyroid (G), and perforated lamellae (PL). The area average of mean curvature, denoted as ⟨H⟩, and the standard deviation of mean curvature, represented as σ_H, for each structure are provided. Reproduced with permission from Ref. [35]. Copyright 2009 American Chemical Society. (c) SCFT-calculated phase diagrams of tapered copolymers with different taper lengths. Reproduced with permission from Ref. [37]. Copyright 2013 American Chemical Society. (d) Phase diagrams of polystyrene-*b*-polypeptoid block copolymers with small junctions having different conformations. Reproduced with permission from Ref. [37]. Copyright 2021 American Chemical Society. (e) Relieved packing frustration of tripod intersections in diblock copolymers by increasing polydispersity index or blending with homopolymers.

stability range was considerably narrower than that observed for triblock copolymer systems [49]. It was evident that triblock copolymer systems offer the more accessible phase window of the *Fddd* structure over a broader range of composition and temperature. This is facilitated by promoting a flat interface between A and B domains, contrary to the favorable curved interface between B and C domains, especially when A and B have nearly symmetric volumes and the composition of B and C is asymmetric.

III. STABILIZATION OF COMPLEX PHASES IN BLOCK COPOLYMERS BY CHAIN CONNECTIVITY REGULATION

A. FK phases in multiblock copolymers

The strategy of linking a greater number of polymer chains in multiblock configurations has led to the discovery of FK phases in block copolymers. FK phases exhibit a distinct arrangement of atoms, characterized by polyhedra with specific arrangements of shared vertices and faces [23]. In metallic

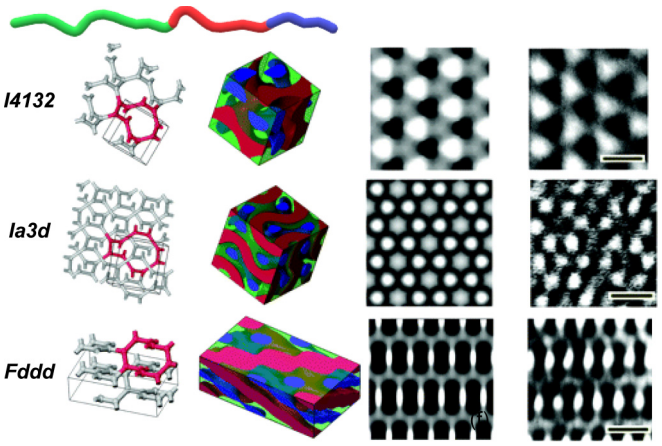

FIG. 2. 3D representations and TEM images of three network structures observed in ABC triblock copolymers. Reproduced with permission from Ref. [45]. Copyright 2004 American Chemical Society.

alloys, a total of 27 FK phases have been identified, while block copolymer systems exhibit a subset of these phases, including the A15 ($Pm\bar{3}\ n$), C14 ($P6_3/mmc$), C15 ($Fd\bar{3}\ m$), and σ phases ($P4_2/mnm$) [Fig. 3(a)]. The σ phase, a type of dodecagonal quasicrystal (DQC), is composed of 30 particles with five distinct types in the unit cell, making it the least symmetric among the four FK structures.

Bates and co-workers identified σ and A15 phases in a polystyrene-*b*-polyisoprene-*b*-polystyrene-*b*-poly(ethylene oxide) (PS-*b*-PI-*b*-PS′-b-PEO) tetrablock copolymer [Fig. 3(b)] [50–52]. Mechanism underlying the stabilization of low-symmetry cubic structures in block copolymer systems was the strong segregation of PEO end blocks from both PS and PI blocks, coupled with the relatively weak segregation between PS and PI, resulting in conformational asymmetry. As illustrated in the bottom panel of Fig. 3(b), the terminal PEO blocks (green) form the core of the spheres, with the PS and PS′ blocks (blue) surrounding these cores to form micelles through forming PI loops or bridges (red). The intermixing of PS and PI chains caused the PS shell to swell, resulting in the formation of a large core-shell structure and an increase in the interfacial area. As a consequence, this preference for a spherical interface fosters the formation of the FK phase.

B. Complex phases in miktoarm or star copolymers

The design of miktoarm and star copolymers has increased the number of methods for controlling microphase separation behavior. Milner and Olmsted provided the first computational insights into the impact of architectural asymmetry on the phase behavior of A_nB_m star copolymers using strong segregation theory analysis [53,54]. Through the introduction of architectural asymmetry in A_nB_m ($n > m$) star copolymers, a more effective stretching of the B domain with fewer segments was anticipated due to the influence of m^2/n^2 values on the effective spring constant of the B block relative to the A block. Furthermore, as the n/m ratio rises, indicating a higher

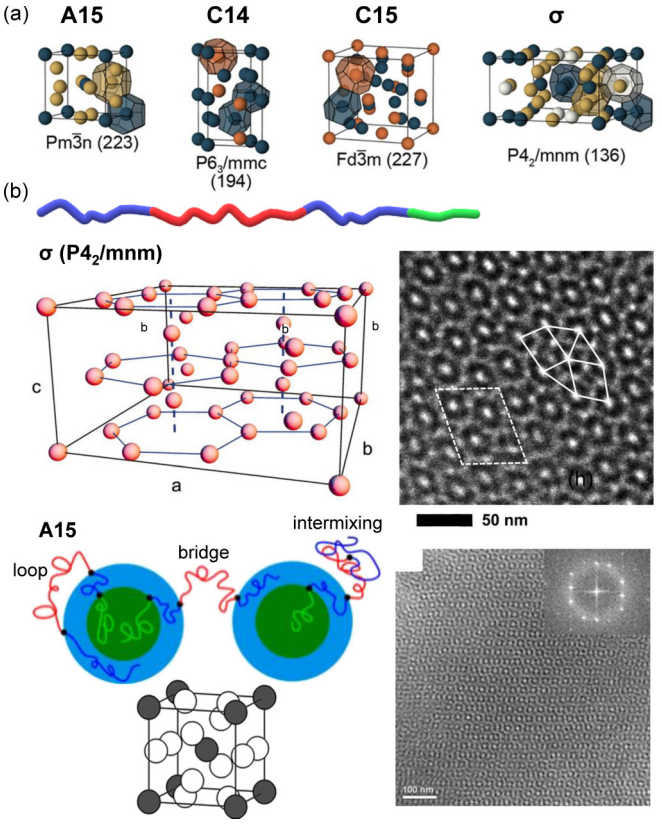

FIG. 3. (a) FK phases observed in block copolymer systems: A15, C14, C15, and σ phases. Reproduced with permission from Ref. [23]. Copyright 2021 American Chemical Society. (b) Unit cell structures and 2D TEM images of σ phase (top) and A15 phase (bottom) derived from ABA′C tetrablock copolymers. Top images reproduced with permission from Ref. [50]. Copyright 2010 American Association for the Advancement of Science. Bottom images reproduced with permission from Ref. [52]. Copyright 2016 American Chemical Society.

degree of branching relative to the linear segments, branched copolymers exhibit a preference for curved interfaces.

Grason *et al.* were the first to theoretically demonstrate the stabilization of A15 phases in diblock copolymers with multiple branches [Fig. 4(a)] [55]. By comparing the phase behavior of A-[B(B_2)]$_2$ block copolymers with that of linear A-B diblock copolymers, these researchers revealed that the multiply branched copolymers with three generations exhibited a considerably broader range of thermodynamically stable A15 structures, attributed to their preference for curved interfaces. The examination of the phase behavior of the AB_n miktoarm star block copolymers in the strong segregation limit revealed the remarkable sensitivity of the AB interface to architectural asymmetry and the increased stability of the A15 phase when the number of B blocks exceeded three [56]. Subsequently, Shi and co-workers revealed the stability of the σ and A15 phases between the bcc and hex ones, with the corresponding phase region expanding with increasing architectural asymmetry [57]. Figure 4(b) shows the phase diagram of AB_4 miktoarm copolymers. These findings have spurred ongoing endeavors to explore the quasicrystalline morphologies of AB-type miktoarm star copolymers.

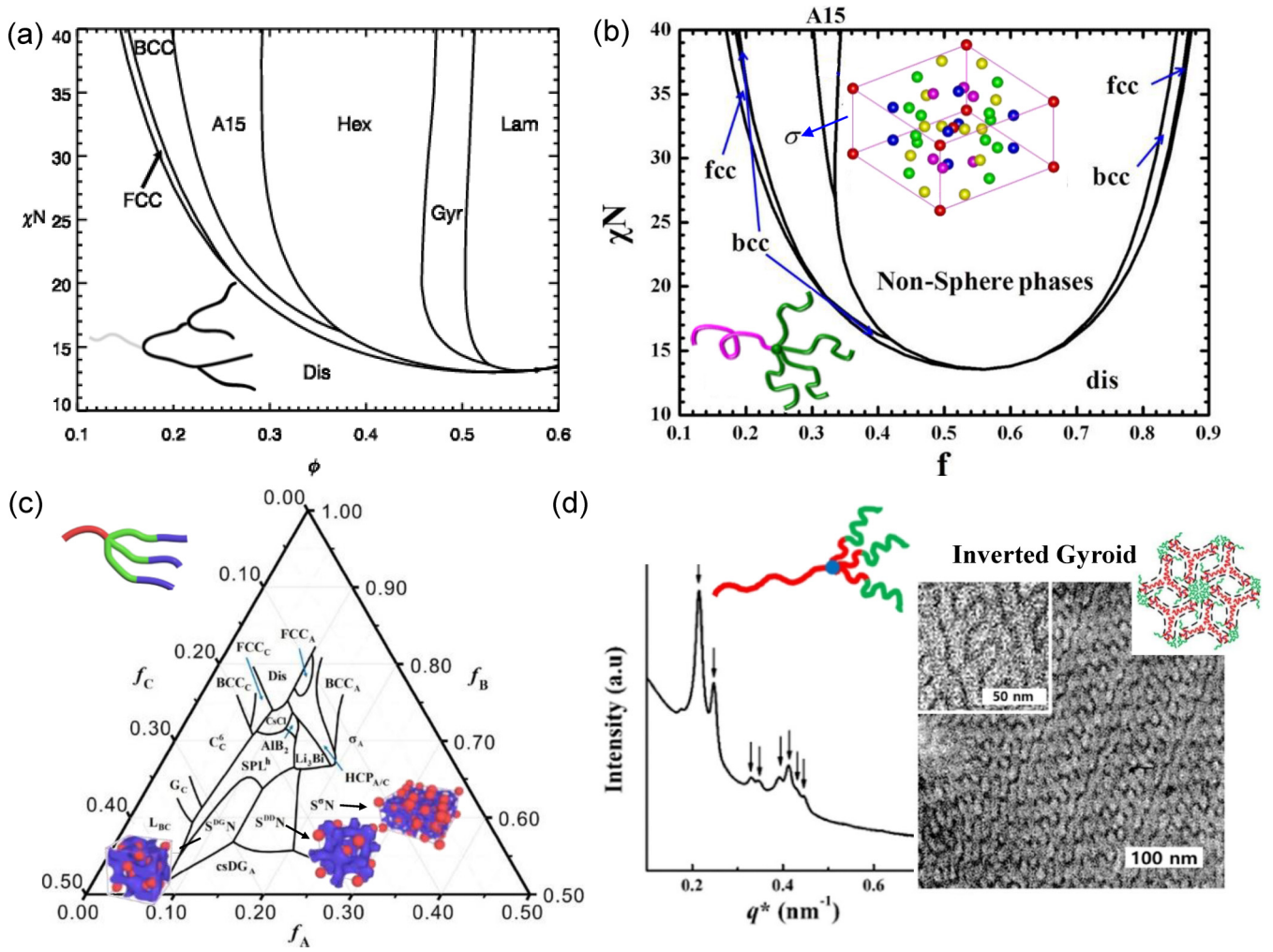

FIG. 4. SCFT-calculated phase diagrams for (a) the three-generation diblocks, revealing the stable phase window of A15 phases, (b) the AB_4 miktoarm star copolymers, showing stability of the σ phase, and (c) the $A(BC)_3$ copolymer with fixed $\chi N = 80$. Reproduced with permission from Refs. [55,57,58]. Copyright 2003 American Physical Society and Copyrights 2014, 2021 American Chemical Society. (d) SAXS profile and TEM image for PS_L-(PS_S-*b*-P2VP)$_3$, representing the formation of inverted gyroid. Reproduced with permission from Ref. [59]. Copyright 2021 American Chemical Society.

Dong and Li investigated the phase behavior of $A(BC)_m$ miktoarm star copolymers by manipulating the architectural asymmetry using SCFT calculations [58]. In contrast to the phase diagram of the ABC linear triblock copolymer, that of the $A(BC)_m$ copolymer ($m = 2$ and 3) displayed a broader range of 3D hybrid morphologies comprising both spherical and network components. Figure 4(c) presents the phase diagram of an $A(BC)_3$ copolymer, where the diamondlike structure is observed to be more stable than the gyroidlike one.

Miktoarm star copolymers provide a unique opportunity to simultaneously adjust architectural and volume-fraction asymmetries. Kim and co-workers demonstrated the formation of inverted gyroid structures in polystyrene-[polystyrene-*b*-poly(2-vinylpyridine)]$_3$[PS_L-(PS_S-*b*-P2VP)$_3$] miktoarm star copolymers when a long PS chain was linked to three short PS-*b*-P2VP chains [Fig. 4(d)] [59]. Longer PS chains were observed farther from the interfaces, which resulted in a radial distribution of PS chains that induced interfacial curvature and alleviated packing frustration.

C. Discovery of FK phases in conformational asymmetric diblock copolymers

Similar to the gyroid structure, which has long been considered as the most thermodynamically stable network structure, the energetically favorable spherical phases in diblock copolymers are considered to adopt a body-centered cubic (bcc) lattice [60]. The SCFT predicts the existence of a limited region of closely packed spheres near the order-disorder transition. However, this consensus was challenged by the discovery of an FK phase in a simple linear diblock copolymer by Bates and co-workers [50]. Prior to this observation, the introduction of architectural asymmetry, typically using copolymers with star and miktoarm architectures [61,62], was a common strategy for achieving topologically close-packed phases.

The SCFT mean-field phase diagram of diblock copolymers reflecting the effects of f and ε showed that the A15 phase is favored around $f_A = 0.3$, between σ and hex morphologies, particularly at high ε (>2.1; Fig. 5) [63]. With increasing ε, the stability of the A15 phase extends

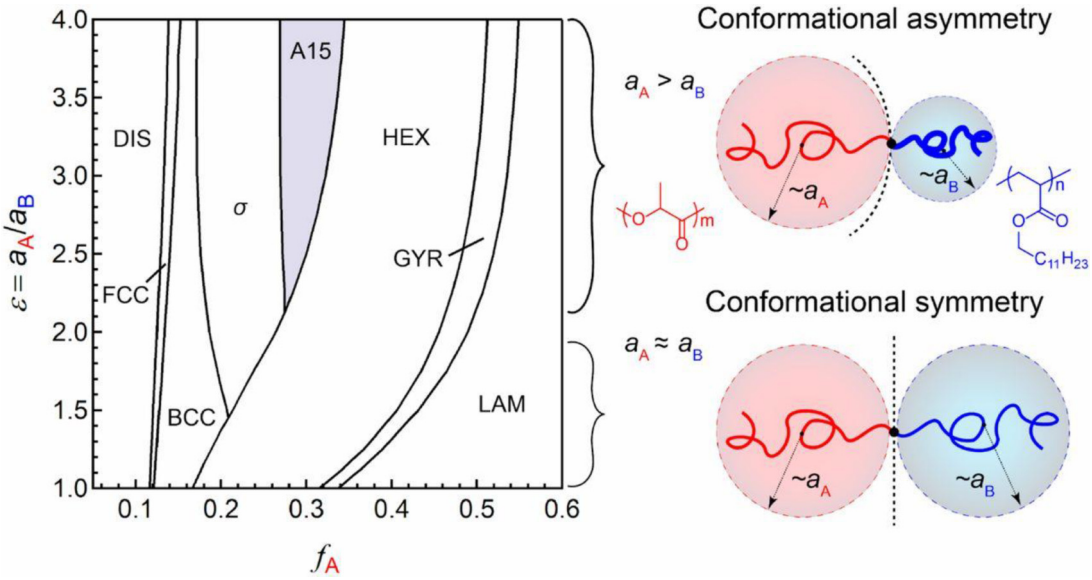

FIG. 5. SCFT mean-field phase diagram of diblock copolymer against f_A and ε. The chemical structure of poly(dodecyl acrylate)-*b*-polylactide having $\varepsilon = 1.85$ is presented in the right panel. Reproduced with permission from Ref. [63]. Copyright 2019 PNAS.

across a wider range of f_A values. This finding is corroborated by the experimental observation of the A15 phase in the poly(dodecyl acrylate)-*b*-polylactide diblock copolymer (PDDA-*b*-PLA; $N = 76$, $f_{PLA} = 0.31$), which is designed to achieve substantial conformational asymmetry ($\epsilon = 1.85$; see chemical structures in the right panel of Fig. 5). The principles dictating the variation of statistical segment lengths in linear diblock copolymers bear resemblance to the observation of complex phases in A_nB_m ($n > m$) star copolymers, achieved by controlling the curvature and swelling behavior of the B domain with fewer segments.

IV. ENGINEERING COMPLEX 3D MORPHOLOGIES IN DIBLOCK COPOLYMERS

A. Configurational regularity

The predominant methods employed to stabilize intricate nanostructures in block copolymers have primarily focused on modifying interfaces or alleviating entropic losses arising from the stretching of polymer chains. However, to achieve a broad spectrum of complex morphologies, it is essential to modify the nearly degenerated free energies of these structures through thermodynamic or kinetic controls.

Hashimoto and Chen and co-workers [64–66] identified thermodynamically stable double diamond (DD) structures in stereoregular diblock copolymers, namely, iso- and syndiotactic polypropylene-*b*-polystyrene [*i*PP-*b*-PS and *s*PP-*b*-PS, respectively; Fig. 6(a)]. This finding is noteworthy, given that triply periodic structures attainable through block copolymers were limited to the gyroid. This approach effectively compensates for the conformational entropy loss resulting from the packing frustration of the minor PP block in the network domains through enthalpic gains due to the formation and association of helical segments.

Small-angle x-ray scattering (SAXS) profile of *s*PP-*b*-PS recorded at 25 °C [Fig. 6(b)] reveals distinct scattering peaks corresponding to the DD structures [64]. Heating to above the melting point of *s*PP (155 °C), resulted in a thermally reversible DD→DG phase transition. The stability of the DD structure is attributed to the interactions among the helical *s*PP segments, which facilitate local arrangement and mesomorphic packing. Consequently, the energy cost of chain elongation is effectively balanced by the energy gain due to helix formation within the microdomains. Although *i*PP-*b*-PS also exhibited thermodynamically stable DD structures and underwent a DG-to-DD transition upon heating, it displayed hysteresis during heating and cooling because *i*PP chain anchoring hindered the translational diffusion of junctions along the interfaces [65]. Transmission electron microscopy (TEM) imaging and 3D TEM tomography revealed the presence of tetrapod intersections in both *s*PP-*b*-PS and *i*PP-*b*-PS [Figs. 6(c) and 6(d)] [65].

Considering the high PDIs of the *i*PP (1.39) and *s*PP (1.32) blocks in the above-mentioned block copolymers, the broad distribution of the PP chain length may help to alleviate packing frustration in tetrapods. Nevertheless, the tetrapod stabilization in diblock copolymers marks a departure from the tripod stabilization observed in high-PDI diblock copolymers, which makes this case unique.

B. Electrostatic control

The difficulty of synthesizing block copolymers with precise regioregularity control or high conformational asymmetry highlights the need to investigate the stabilization of unique 3D structures through noncovalent interactions in equilibrium [67]. Copolymers containing charged units are promising candidates because of their adjustable chain sizes, which are regulated by the strength of the intermolecular interactions. Furthermore, by adding ionic additives to polymers containing charged moieties in their backbones, the adjustability in electrostatic interactions can be increased through

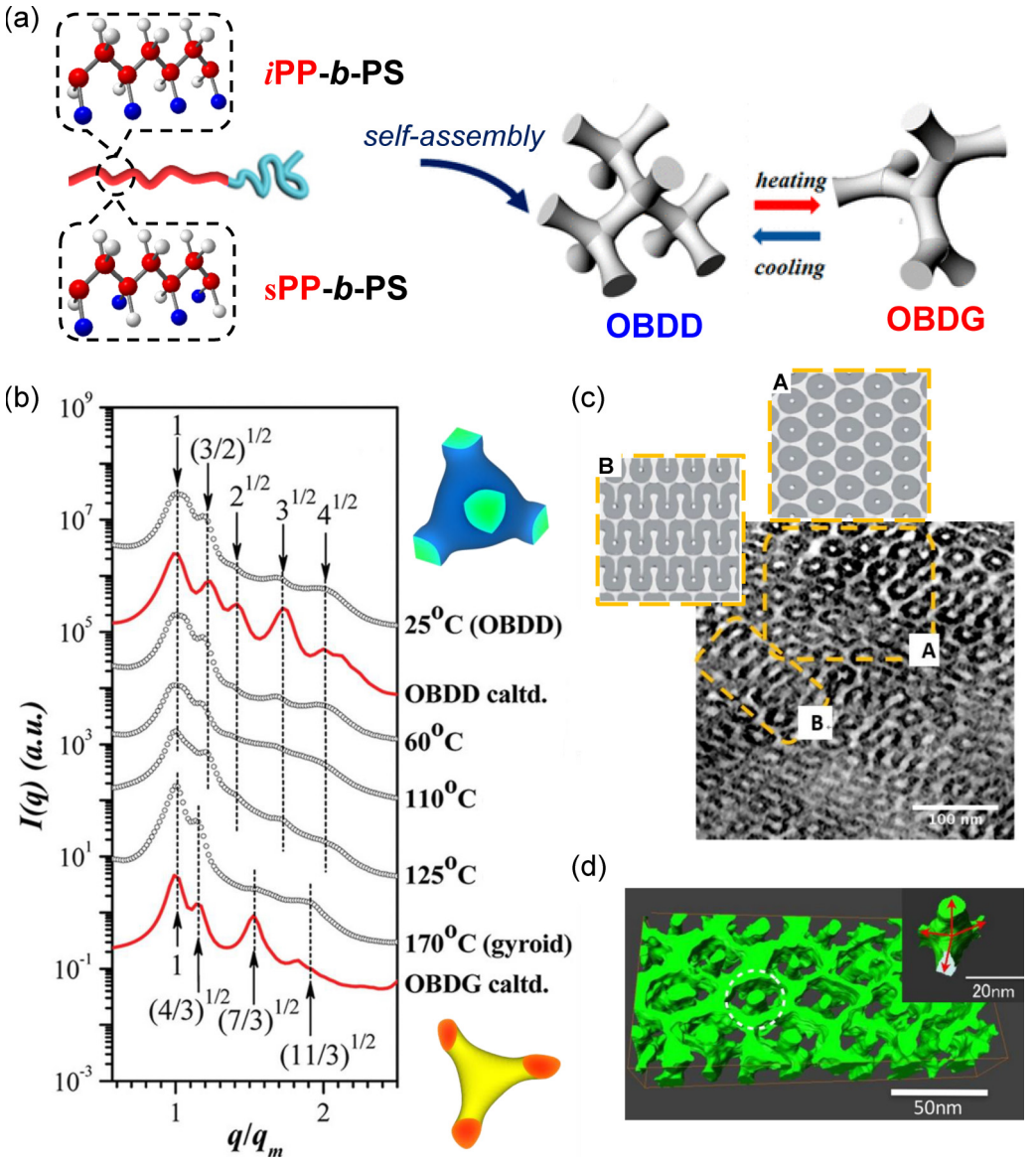

FIG. 6. (a) Schemes depicting phase transition between the ordered bicontinuous double diamond (OBDD) and ordered bicontinuous double gyroid (OBDG) structures in *i*PP-*b*-PS and *s*PP-*b*-PS block copolymers. Reproduced with permission from Ref. [65]. Copyright 2018 American Chemical Society. (b) Temperature-dependent SAXS profiles of *s*PP-*b*-PS. Reproduced with permission from Ref. [64]. Copyright 2012 American Chemical Society. (c) TEM image and (d) TEM tomograms of *i*PP-*b*-PS. The regions A and B in (c) can be simulated by the projections from the [111] and [211] directions of the OBDD lattice, respectively. Reproduced with permission from Ref. [65]. Copyright 2018 American Chemical Society.

variations in the types and compositions of ions. Both experimental [68] and theoretical [69] studies have demonstrated the significance of electrostatic interactions in the charged domains for manipulating the phase diagrams of the corresponding block copolymers. The precise control of these long-range interactions can be accomplished by selectively introducing ionic salts within the ionic domains. This approach holds promise for tailoring the properties of polymer electrolytes and making them highly suitable for energy storage and conversion applications [70,71].

Park and co-workers investigated the phase behavior of acid-functionalized polystyrene-poly(methylbutylene) block copolymers by controlling the electrostatic interactions in their ionic domains through (1) the variation of ionic liquid (IL) type [72], (2) IL nonstoichiometry adjustment [73], and (3) the chemical modification of the acid functional groups in the polymers [74]. The introduction of different ILs into the sulfonated polystyrene-poly(methylbutylene) (PSS-*b*-PMB) block copolymer leads to diverse ordered morphologies [Fig. 7(a)] [72]. With the use of the same IL anion [bis(trifluoromethanesulfonyl)imide ([TFSI])], varying cations as pyrazolium ([Py]) and 2-methylimidazolium ([2MIm]) resulted in the formation of equilibrium lam structures at room temperature, which transitioned to disordered phases upon heating. In contrast, hex structures were formed when imidazolium ([Im]) and 1-methylimidazolium ([1MIm])

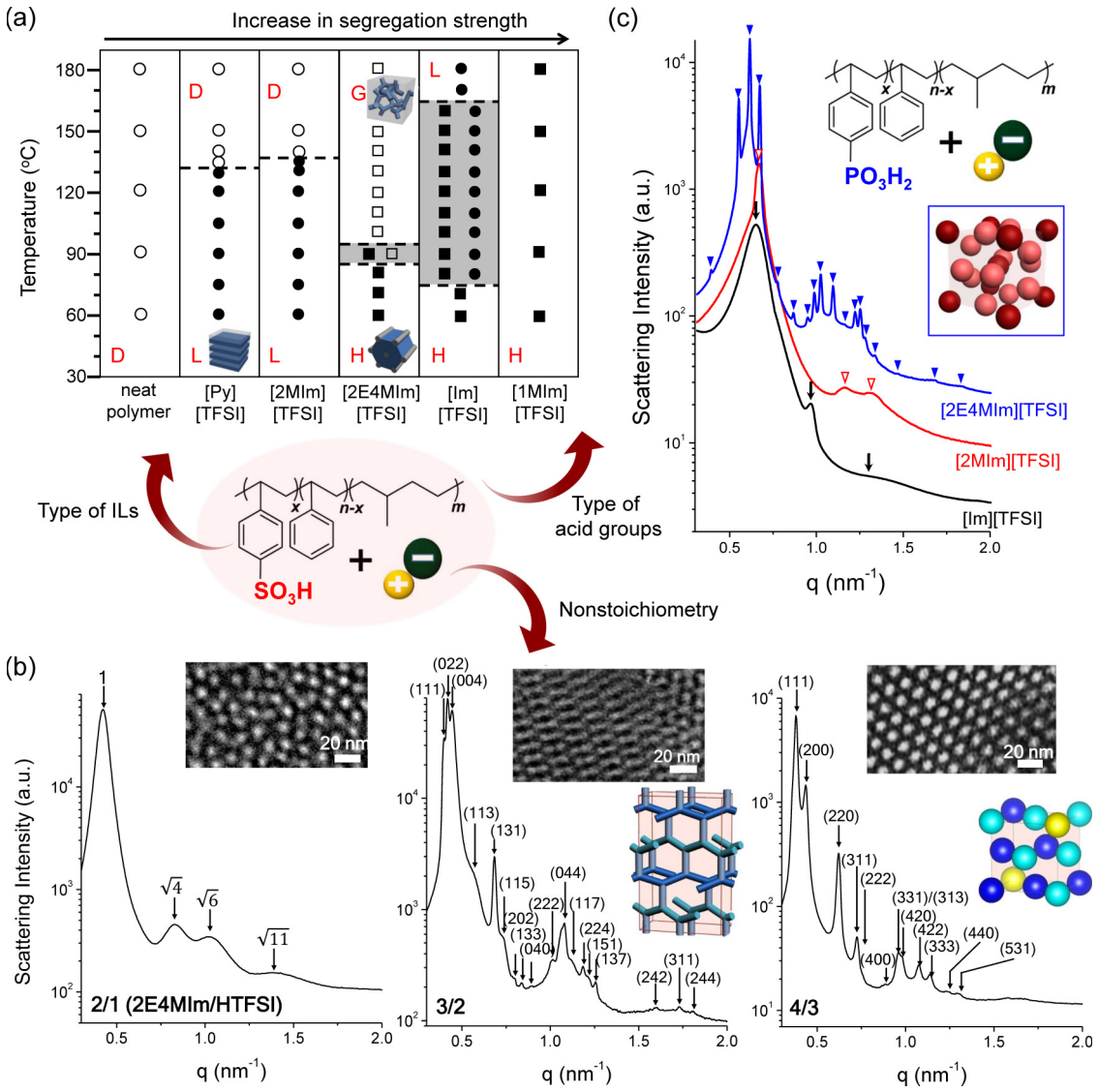

FIG. 7. (a) Phase diagrams of PSS-*b*-PMB block copolymer comprising different ILs. D, L, H, and G indicate disorder, lam, hex, and gyroid morphology, respectively. The coexistence phases are shown by shadows. Reproduced with permission from Ref. [72]. Copyright 2012 American Chemical Society. (b) SAXS profiles of PSS-*b*-PMB block copolymer comprising 2E4MIm/TFSI for compositions of 2/1, 3/2, and 4/3. The arrows (↓) represent the series of Bragg peaks of each sample, as indexed in the figure. Reproduced with permission from Ref. [73]. Copyright 2016 American Chemical Society. (c) SAXS profiles of PSP-*b*-PMB block copolymer comprising various ILs: Bragg peaks at $1q^*$, $\sqrt{2}q^*$, $\sqrt{4}q^*$ (↓, [Im][TFSI], bcc); $1q^*$, $\sqrt{3}q^*$, $\sqrt{4}q^*$ (▽, [2MIm][TFSI], hex; and those corresponding to A15 phase (▼, [2E4MIm][TFSI]). Reproduced with permission from Ref. [74]. Copyright 2016 John Wiley and Sons.

cations are used. Although [Im] and [Py] (as well as [1MIm] and [2MIm]) cations have comparable van der Waals volumes, the diazole ring structures affect the strength of the ionic interactions in the PSS domains, leading to differences in morphology. Alkylation at the protic position of [Im] to afford [1MIm] results in a highly segregated hex structure owing to substantial chain stretching. The introduction of 2-ethyl-4-methylimidazolium ([2E4MIm]) with two alkyl substituents at protic positions resulted in an analogous hex structure at room temperature, which transitioned to a gyroid phase around 90 °C.

In the second approach, a set of ILs based on [2E4MIm][TFSI] is introduced into the PSS-*b*-PMB block copolymer by varying the 2E4MIm/HTFSI molar ratio, with the representative SAXS profiles and TEM images of such samples shown in Fig. 7(b) [73]. The appearance of an *Fddd* structure in diblock copolymers is a rare phenomenon attributed to the considerable stretching of charged PSS chains caused by the adjustable strength of electrostatic interactions with embedded ILs. This interaction directly affects the extent of segregation between the PSS and PMB blocks.

In the third approach, Park and co-workers investigated the morphology and thermodynamics of phosphonated poly(styrene-*b*-methylbutylene) (PSP-*b*-PMB) block copolymers containing different ILs [74]. By changing the acid functional groups from $-SO_3H$ to $-PO_3H_2$, it was aimed to enhance the molecular interactions between the IL cations and the acid functional groups of the polymers, as pre-

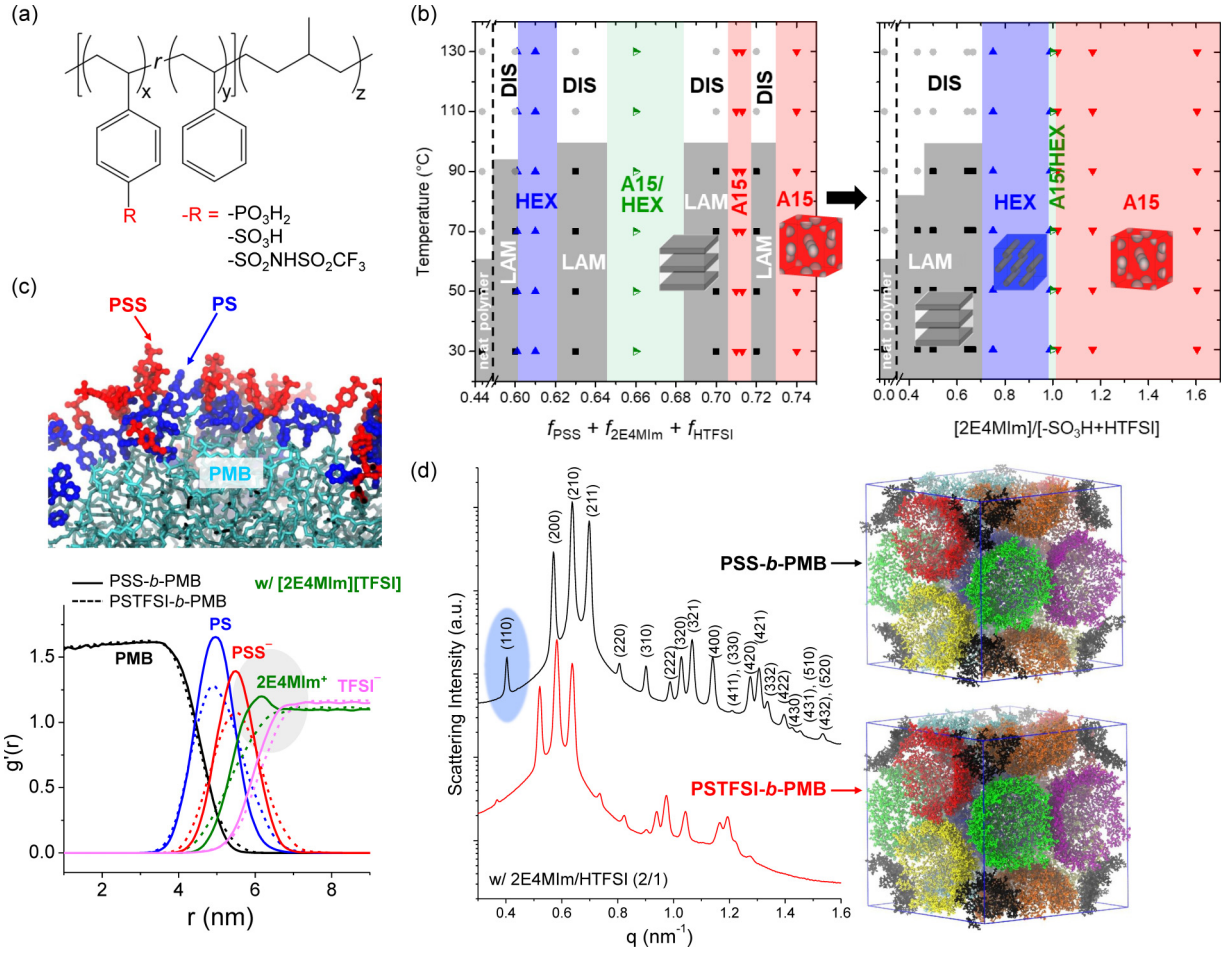

FIG. 8. (a) Chemical structures of acid-functionalized polystyrene-*b*-poly(methylbutylene) block copolymers. (b) Phase diagrams of PSS-*b*-PMB comprising nonstoichiometric 2E4MIm/HTFSI against the volume fraction of ionic phases (left) and the molar ratio of 2E4MIm to total acid moieties (right). (c) MD simulation results of a PSS-*b*-PMB micelle dissolved in 2E4MIm/HTFSI, including radial distribution of each species from the center of the PMB core. (d) SAXS profiles of PSS-*b*-PMB and PSTFSI-*b*-PMB comprising 2E4MIm/HTFSI (2/1), alongside MD simulation snapshots showing dissimilar A15 structures. Reproduced with permission from Ref. [75]. Copyright 2021 The Authors.

dicted by density functional theory calculations. These endeavors marked the first observation of equilibrium A15 phases in linear diblock copolymers [Fig. 7(c)]. The observed phase sequences (bcc with [Im][TFSI] and A15 with [2E4MIm][TFSI]) can be rationalized by the enhanced thermodynamic compatibility between the [2E4MIm] cations and PSP chains, aided by favorable hydrophobic interactions. Theoretical calculations suggest that the A15 phase is more stable in the strong segregation regime than the bcc phase. When PSP-*b*-PMB with slightly higher N values was used, the A15 lattice was detected for both [2MIm][TFSI] and [2E4MIm][TFSI], which further affirmed the enhanced thermodynamic stability of A15 structures within a high-χN regime of block copolymer phase diagrams.

The phase behavior of block copolymers can be efficiently controlled by adjusting the number of charged units therein. Park and co-workers investigated the phase behavior of acid-functionalized block copolymers with different types of tethered acid groups [Fig. 8(a)] [75]. Figure 8(b) presents the phase diagrams of PSS-*b*-PMB containing nonstoichiometric 2E4MIm/HTFSI, revealing a weak dependence on the volume fraction of the ionic domains and the occurrence of unprecedented "reentrance" phase sequences. Specifically, even a slight change in the volume fraction of the ionic phases leads to a morphological shift from the lam phase to A15, which cannot be explained by conventional block copolymer phase diagrams. The molar ratio of 2E4MIm to the total acid groups [right panel of Fig. 8(b)] strongly influences the copolymer morphology. A15 phases emerge with increasing 2E4MIm content, which indicates elevated stability owing to the enhanced electrostatic interactions in the ionic domains.

This behavior is in stark contrast to the phase diagram of sulfonyl(trifluoro methanesulfonyl)imide-functionalized polystyrene-*b*-poly(methylbutylene) (PSTFSI-*b*-PMB), which reveals the occurrence of sequential lam→hex→spherical phase transitions with the increasing volume fraction of the ionic domains. The dissimilarity between PSS-*b*-PMB and PSTFSI-*b*-PMB was elucidated using molecular dynamics (MD) simulations [Fig. 8(c)], which revealed contrasting $2E4MIm^+$ distributions near the micellar interface. In PSS-*b*-PMB, $2E4MIm^+$ is concentrated near the PSS^- chains, indicating the formation

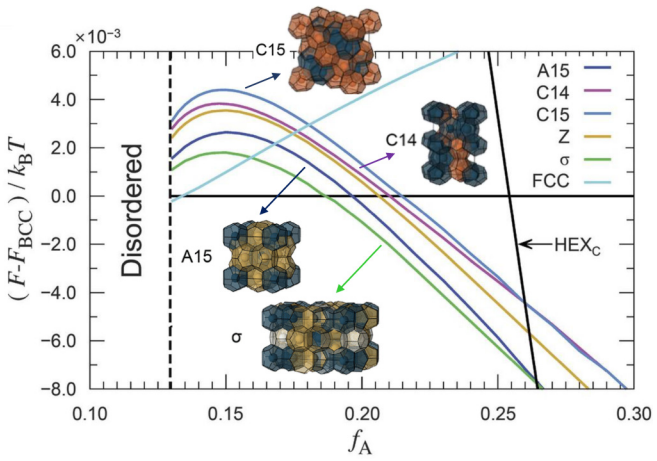

FIG. 9. Free-energy difference between various Frank-Kasper phases with respect to bcc as a function of f_A for $\chi N = 40$ and $\varepsilon = 2$. Reproduced with permission from Refs. [23,77]. Copyright 2021 American Chemical Society and Copyright 2017 American Association for the Advancement of Science.

of ionic shells. This phenomenon was not observed in PSTFSI-*b*-PMB.

The impact of the formation of the PSS^-/2E4MIm$^+$ interfacial layer on the stability of the A15 phase was revealed by the strong scattering intensity of the (110) peak of PSS-*b*-PMB [Fig. 8(d)]. As illustrated in the MD simulation snapshots in the right part of this figure, the A15 unit structure created using PSS-*b*-PMB exhibits sharp micellar interfaces with reduced concentration fluctuations.

C. Kinetic controls

Kinetically trapping specific metastable states of block copolymers through supercooling from disordered states or rapid casting from particular solvents is referred to as kinetic control. Despite its thermodynamic instability, this method is appealing for creating unique morphologies in block copolymers. Some of these structures can exhibit prolonged stability, thereby offering potential practical utility across various applications.

For example, two blocks with significantly different statistical segment lengths (b) were prepared to introduce interfacial curvature into low-symmetry structures in diblock copolymers and thus create conformational asymmetry ($\varepsilon = b_A/b_B > 1$) [76]. As a result, the σ phase was obtained in a polyisoprene-*b*-polylactide diblock copolymer (PI-*b*-PLA) with ε (b_{PLA}/b_{PI}) = 1.15. Metastable C14 and C15 Laves phases were generated by controlling the thermal history of PI-*b*-PLA [77]. The results of SCFT free-energy calculations on diblock copolymers with conformational asymmetry ($\varepsilon = 2$; Fig. 9) show that FK phases become thermodynamically favored near the phase boundary between bcc and hex structures. Although the σ phase is most stable, the minimal free-energy difference with other phases enables the transition to nonequilibrium FK phases via precise kinetic control.

Recent studies have brought attention to instances where packing frustration in linear block copolymers was relieved by employing solvents to stabilize various curvatures. Ho and co-workers realized a diverse range of 3D network structures [78], including DG, DD, and double primitive (DP; Schwarz P surface) phases, using a single polystyrene-*b*-polydimethylsiloxane (PS-*b*-PDMS) block copolymer forming a lam phase [79]. Although these structures are acknowledged to be in a nonequilibrium state, it is crucial to highlight that this work revealed the first instance of DP structures in any linear diblock copolymers. The key to this achievement was the variation of the solvent evaporation rate, with fast solvent evaporation leading to a mixture of DD (minor) and DP (major) structures [Fig. 10(a)].

The coexistence of these structures was confirmed by TEM, with the representative TEM images of the DG, DD, and DP structures shown in Fig. 10(b). The stabilization of the DP structure, characterized by bulky hexapod intersections with high-packing frustration, is particularly noteworthy. This finding marks the experimental occurrence of P surface in block copolymers, which is attributed to the facile chain stretching of PDMS blocks that enables extension into the interior core of the junctions and helps to maintain the kinetically trapped state after rapid solvent evaporation.

Given that the DP structure was formed in a nonequilibrium state through kinetic control, heating induced a structural transition into the DG structure to reduce packing frustration. Figure 10(c) presents the transitions between the above network structures, revealing that the hexapod (P surface) structure undergoes stretching in the [111] direction to afford a tetrapod (D surface). Subsequently, a similar process occurs in the [100] direction, resulting in the development of a tripod (G surface). This discovery implies that conditions promoting the substantial stretching of polymer chains in minor domains enable the exploration of diverse network structures in linear block copolymers, overcoming the challenges posed by packing frustration. The introduction of different solvent mixtures might further complicate observations, necessitating the exploration of various scenarios for 3D network structures.

V. INSIGHTS FROM SUPRAMOLECULAR ASSEMBLY AND SURFACTANT ASSOCIATION

A. Key role of molecular interactions and linker structures

Although 3D network structures with high-packing frustration are rare in block copolymers, they are more common in solvent-free liquid crystals [80,81]. Tschierske *et al.* revealed various network structures, e.g., DG, DD, single diamond (SD), and single primitive (SP) structures, in rodlike amphiphiles with branched side chains [82–85]. The length and branch number of the space-filling lateral chains could be adjusted to precisely control dV/dr [Fig. 11(a)] and thus stabilize a variety of network structures [86]. In addition, the design of end groups capable of hydrogen bonding and establishing strong cohesive aggregates at the convergence points of network channels is also crucial for reducing packing frustration.

The pioneering work of Cheng and co-workers on the self-assembly of giant amphiphiles revealed an unconventional phase behavior [87–89]. The tailored molecular designs of amphiphiles with polyhedral diol-functionalized oligomeric silsesquioxanes (DPOSS) as hydrophilic heads and PS chains

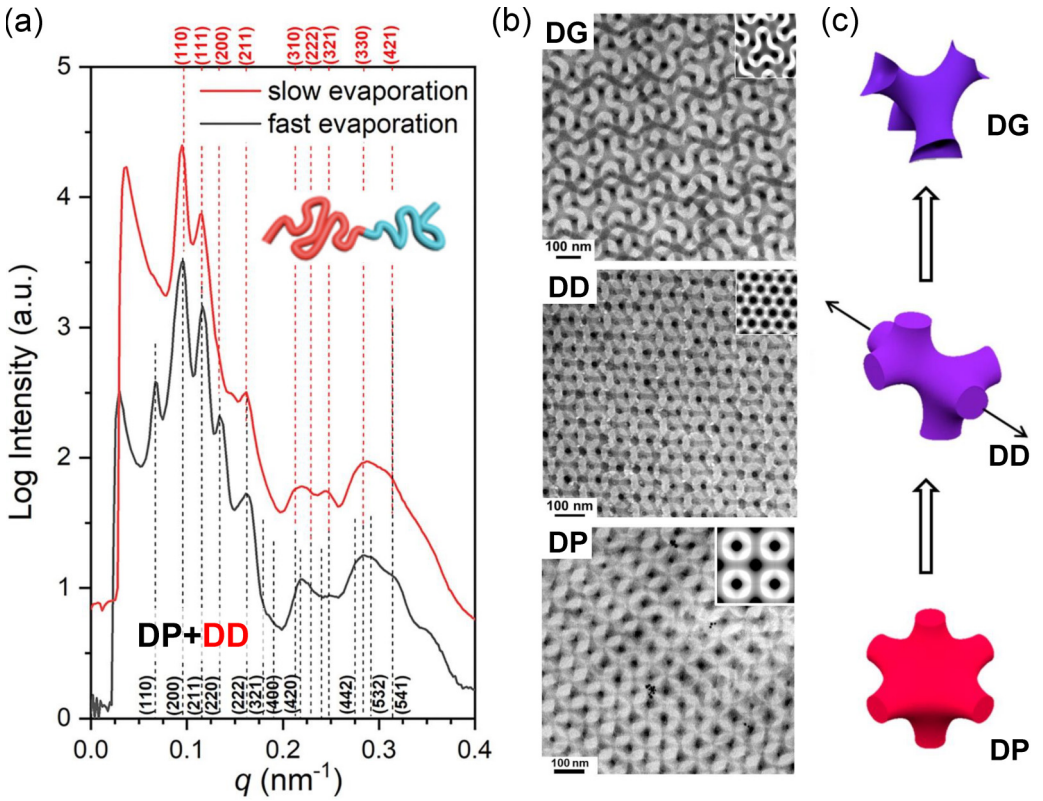

FIG. 10. (a) SAXS profiles of PS-*b*-PDMS, obtained by different evaporation rates of solvent. (b) TEM images of double gyroid (DG), double diamond (DD), and double primitive (DP) structures. (c) Schematic illustration of the pulling-apart process of hexapod to tetrapod, and to tripod. Reproduced with permission from Ref. [79]. Copyright 2021 PNAS.

as hydrophobic tails resulted in the formation of FK and quasicrystal phases [88]. Figure 11(b) presents the phase diagram of DPOSS-nPS$_m$ with different PS volume fractions ($n = 1 - 4$), revealing the formation of A15, σ phases, and DQCs at $n = 3$. The FK phase window broadens upon going to $n = 4$, which aligns with the appearance of FK phases in the star and miktoarm polymers. Dendritic architectures create curved interfaces, which stabilize the FK phases relative to their linear counterparts with similar molecular weights and compositions. The bottom panel presents the representative SAXS profiles of DPOSS-4PS$_{10}$, DPOSS-4PS$_{13}$, and DPOSS-4PS$_{15}$, highlighting the stabilization of the A15, σ, and DQC phases, respectively.

Cheng and co-workers precisely adjusted the alkyl linkages connecting (i) the perylene bisimide (PBI) core and amide group and (ii) the phenyl and triazole groups to further examine the effects of linker structure on the phase behavior of giant amphiphiles [Fig. 11(c)] [89]. A15 and σ phases were produced by the self-assembly of the supramolecular structures in PBI-C1-6BP and PBI-C3-6BP, respectively. The deformation degree of the spherical motifs increased with the increasing length of the relatively flexible alkyl amide linker, which favored the formation of bcc structures. This finding highlights the potential of linker chemistry for controlling the microphase separation behavior of amphiphiles and block copolymers in a broader context.

VI. DEVELOPMENT OF COMPLEX 3D STRUCTURES FROM LINEAR DIBLOCK COPOLYMERS USING END-GROUP CHEMISTRY

A. Interfacial curvature manipulation based on end-group attachment

The unique self-assembly of amphiphiles signifies the importance of block copolymer termini for determining phase behavior. Since the early 1990s, researchers have focused on modifying the termini of homopolymers and block copolymers by incorporating specific functional groups to adjust rheological properties [90] and the order-disorder transition temperature [91,92]. Nevertheless, the influence of block copolymer termini on self-assembly behavior has not been carefully considered, mainly because these termini constitute a small fraction (<1%) of the entire block copolymer structure.

In 2013, Park and co-workers introduced the "one is enough" approach by demonstrating the formation of diverse self-assembled morphologies in a single polystyrene-*b*-poly(ethylene oxide) (PS-*b*-PEO) block copolymer [93]. The TEM images in Fig. 12(a) indicate that the attachment of $-SO_3H$ or $-SO_3Li$ end groups to PS-*b*-PEO increases the extent of segregation between the PS and PEO blocks and introduces a certain curvature to stabilize the hexagonal structures in a nominally symmetric composition. The introduction of a minimal amount of lithium salts further strengthens

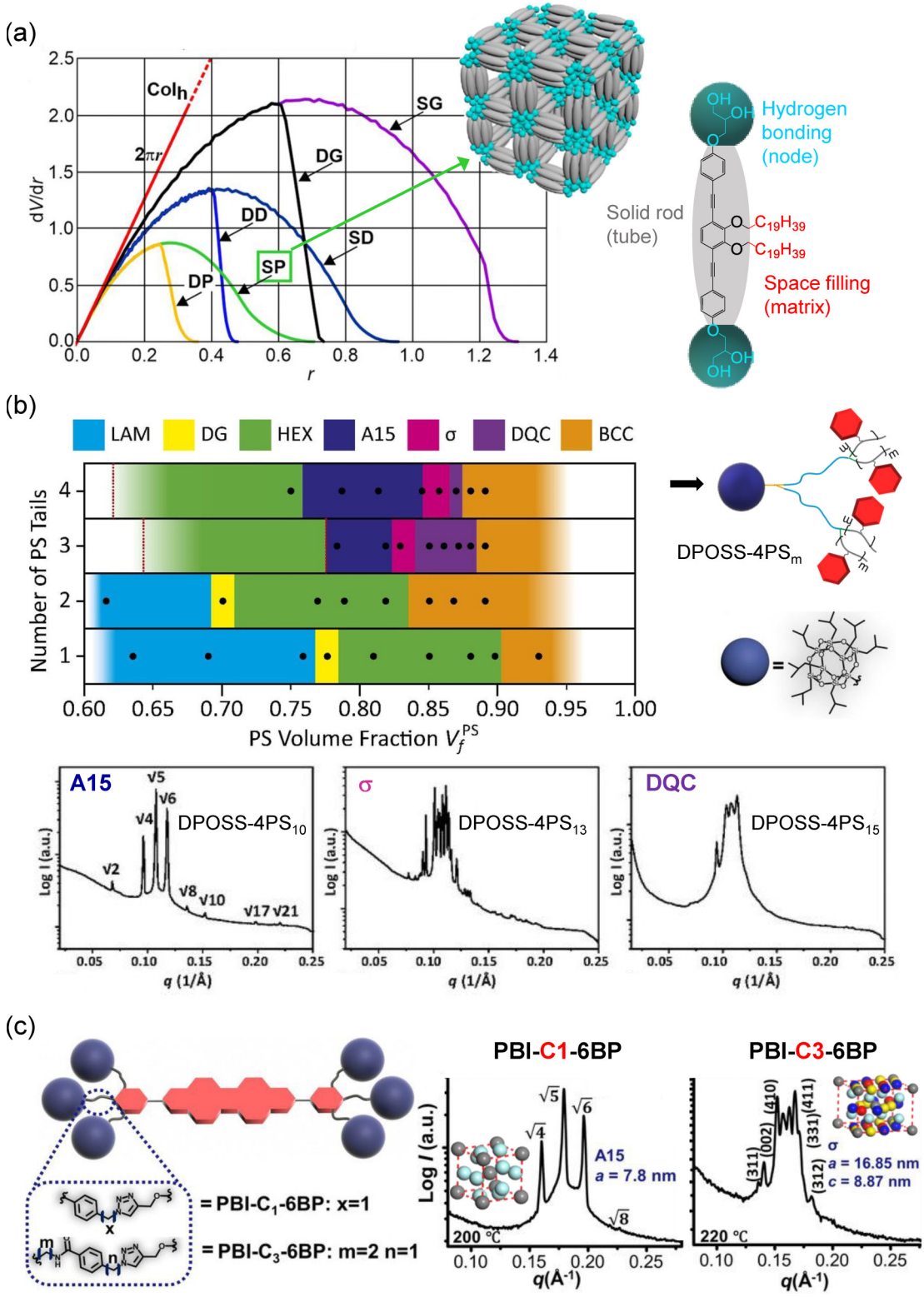

FIG. 11. (a) Radial volume distribution dV/dr curves presented for each cubic phase, with tunable dV/dr based on the number of space-filling chains. The $2 \times 2 \times 2$ unit cells of the single primitive structure consisting of rodlike amphiphiles are illustrated. Reproduced with permission from Ref. [85]. Copyright 2020 American Chemical Society. (b) Phase diagram of DPOSS-nPS$_m$ giant amphiphiles comprising different number of PS tails against PS volume fraction. SAXS profiles of three representative DPOSS-4PS$_m$ samples showing the A15 phase, σ phase, and DQC phase are shown in the bottom panel. Reproduced with permission from Ref. [88]. Copyright 2016 PNAS. (c) Self-assembled supramolecular structures of PBI-C$_n$-6BP with linkage structure variations. SAXS profiles of PBI-C$_1$-6BP and PBI-C$_3$-6BP displaying A15 phase and σ phase, respectively, are shown. Reproduced with permission from Ref. [89]. Copyright 2020 John Wiley and Sons.

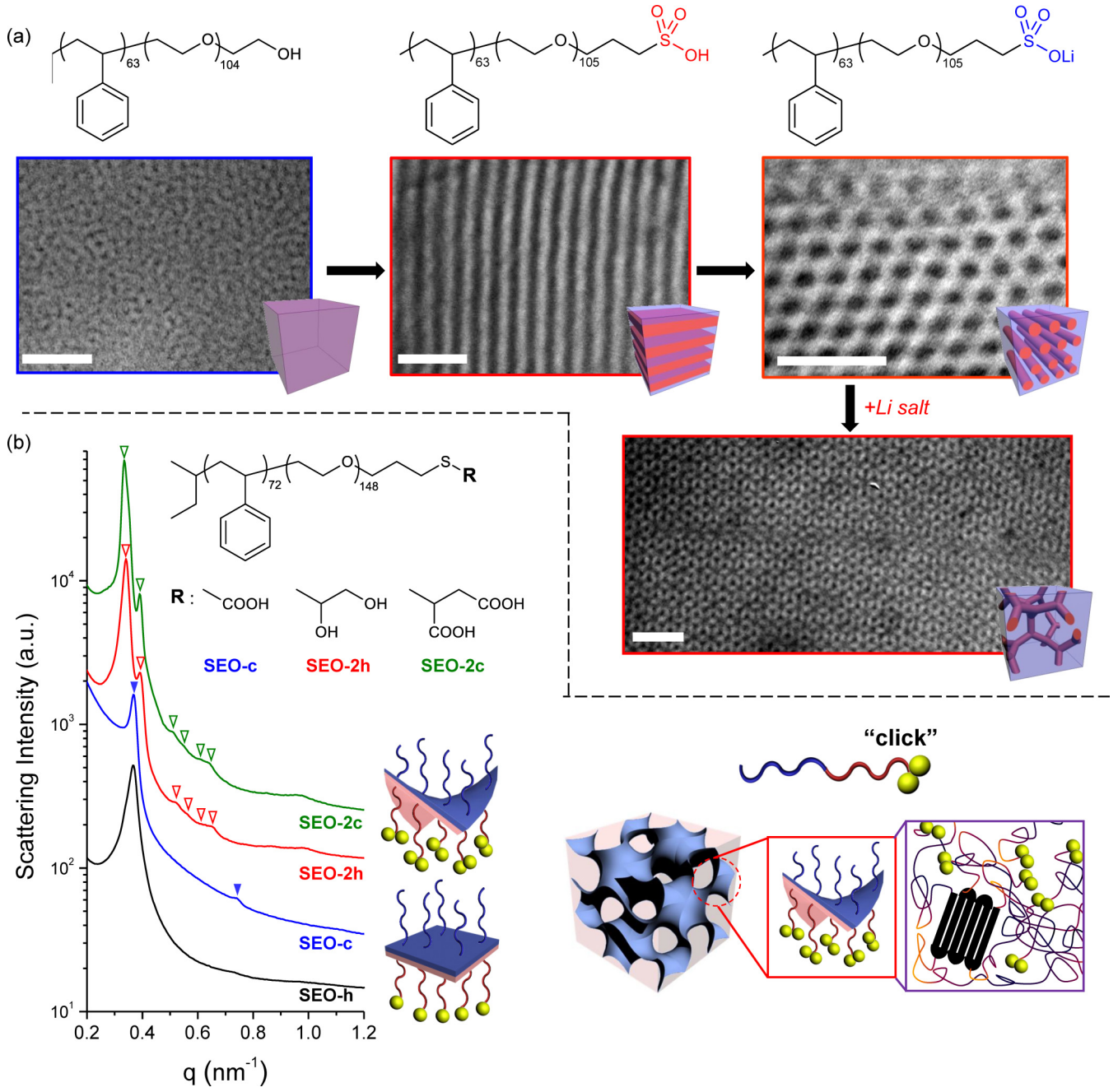

FIG. 12. (a) Chemical structures and TEM images of pristine PS-*b*-PEO and end-functionalized PS-*b*-PEOs with sulfonate groups. The bottom panel displays a TEM image of LiTFSI-doped PS-*b*-PEO-SO_3Li ($r = 0.02$). Reproduced with permission from Ref. [93]. Copyright 2013 American Chemical Society. (b) Chemical structures and SAXS profiles of end-functionalized PS-*b*-PEOs with monofunctional and difunctional moieties. The diagram on the right illustrates the interfacial curvatures and decreased PEO crystallinity in di-end-functionalized PS-*b*-PEO. Reproduced with permission from Ref. [94]. Copyright 2017 American Chemical Society.

end-group-driven molecular interactions and stabilizes DG structures.

In a follow-up study focused on enhancing end-group interactions, Park and co-workers introduced diol and dicarboxylic acid end groups into PS-*b*-PEO using thiol-ene click chemistry [Fig. 12(b)]. This allowed the creation of DG structures in PS-*b*-PEO with nearly symmetric compositions, eliminating the necessity to screen block composition to identify a specific value for stabilizing the triply periodic minimal surfaces [94]. Given that end-group chemistry is remarkably simple compared to the elaborate synthetic processes required for copolymers with complex architectures, this finding is highly important.

This morphological transformation was accompanied by a substantial decrease in the PEO chain crystallinity, thereby increasing the PEO free volume and altering the PEO chain conformation. The proposed mechanism involves the di-end functional groups promoting terminal aggregation via strong hydrogen bonding, which leads to an enthalpic gain that can overcome entropic losses due to chain stretching and thus

effectively alleviate packing frustration without the need for additives.

B. Role of termini distribution in stabilizing 3D structures with high-packing frustration

Grason and co-workers theoretically examined end-group distributions in DG network structures and established skeletal (the central points within tubular domains in one-dimensional lines) and medial packing [the set of points arranged on two-dimensional (2D) surfaces] boundaries using a geometric approach to describe the strong stretching in block copolymer melts [Fig. 13(a)] [95]. By comparing the thermodynamics of medial packing with that of skeletal packing in the DG phase, the authors showed that the free energy per chain was substantially lower in the former packing because of the reduced stretching of the minor block therein. This entropic gain is crucial for the structural stability of the DG structure over hex structures in strongly segregated melts [Fig. 13(b)]. The inset of Fig. 13(b) presents the calculated block entropies at equal intermaterial dividing surface (IMDS) areas per chain (S_α).

The same group employed the medial strong segregation theory to reevaluate the thermodynamics of cubic network formation in strongly segregated diblock melts, relating chain packing environments to the medial geometry of tubular network surfaces [96,97]. Medial packing motifs are crucial for stabilizing complex morphologies with high-packing frustration, such as DD and DP structures. Figure 13(c) illustrates the distribution of the free energy per chain, showing the dominance of the enthalpic component with maximal enthalpic costs in the elbow regions of the DG nodes. In contrast, for the DD and DP nodes, the maximal enthalpy and stretching entropy costs occur halfway along the struts and on the monkey saddles of the IMDS, respectively.

The net free energies of the DD and DP structures were the smallest in the elbow region, with high packing costs arising from both entropic and enthalpic contributions. Although DG structures are traditionally deemed more stable because of their larger terminal web surface areas, the DD and DP structures exhibited a substantial decrease in free energy based on the end-group distribution, which suggested experimental directions for future exploration.

C. End-group and linker chemistries as directions for future research on block copolymer self-assembly

Park and co-workers discovered thermodynamically stable plumber's nightmare structures in linear block copolymers by introducing different end groups and linkers connecting them to the polymer chains [98]. Two PS-*b*-PEO diblock copolymers with symmetric and asymmetric block compositions were synthesized. The hydroxyl terminal of PS-*b*-PEO was converted to a diol or primary amine group, and diphosphonic acid (*d*PA) end groups were then attached using different linker molecules. These *d*PA-endedPS-*b*-PEOs were named SEO-*N*-*d*PA (amine linker) and SEO-*O*-*d*PA (ether linker) [Fig. 14(a)]. For SEO-*N*-*d*PA, a mixture of *Fddd* and $Ia\bar{3}$ *d*

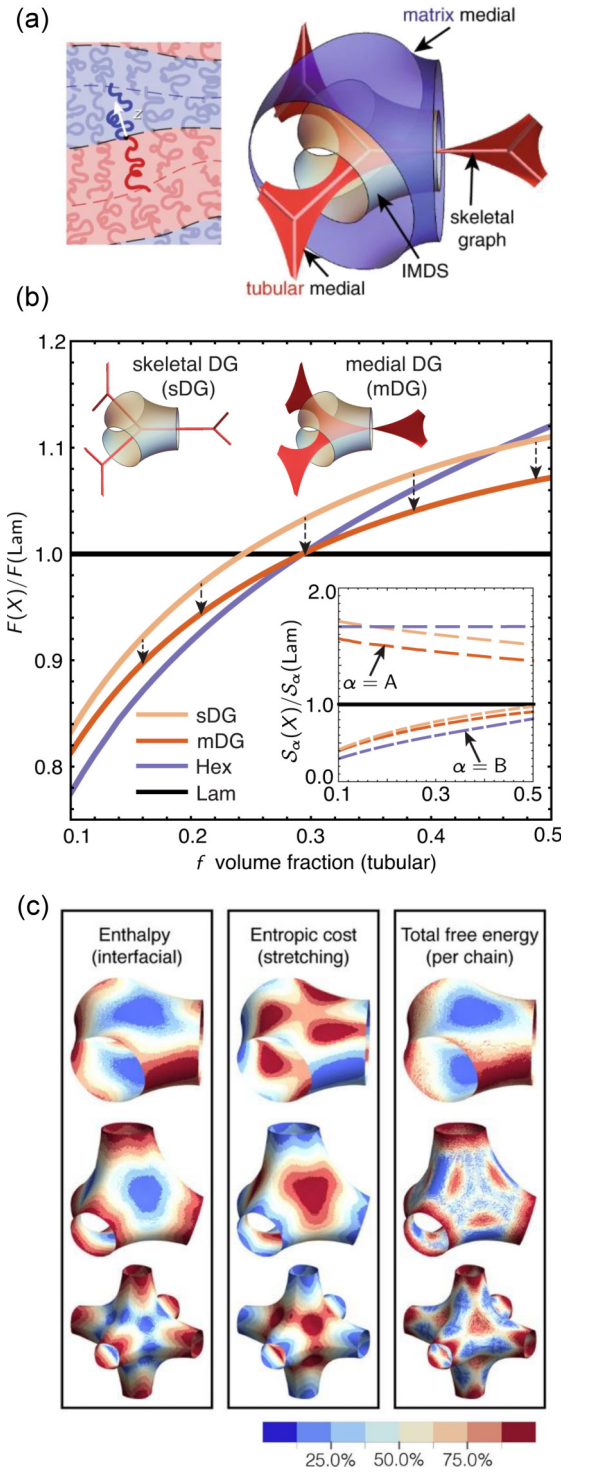

FIG. 13. (a) Schematic drawings of medial surface and skeletal graph of tubular blocks. (b) Comparison plot of free energy for medial-DG (mDG) and skeletal-DG (sDG) to hex and lam phases. Reproduced with permission from Ref. [95]. Copyright 2021 The Authors. Published by Springer Nature under a Creative Commons Attribution License (CC BY 4.0). (c) Enthalpy, entropic cost, and local free energy per chain contributions, mapped onto the IMDSs of the network phases for an elastically symmetric case with $f \approx 0.29$. Reproduced with permission from Ref. [96]. Copyright 2023 American Chemical Society.

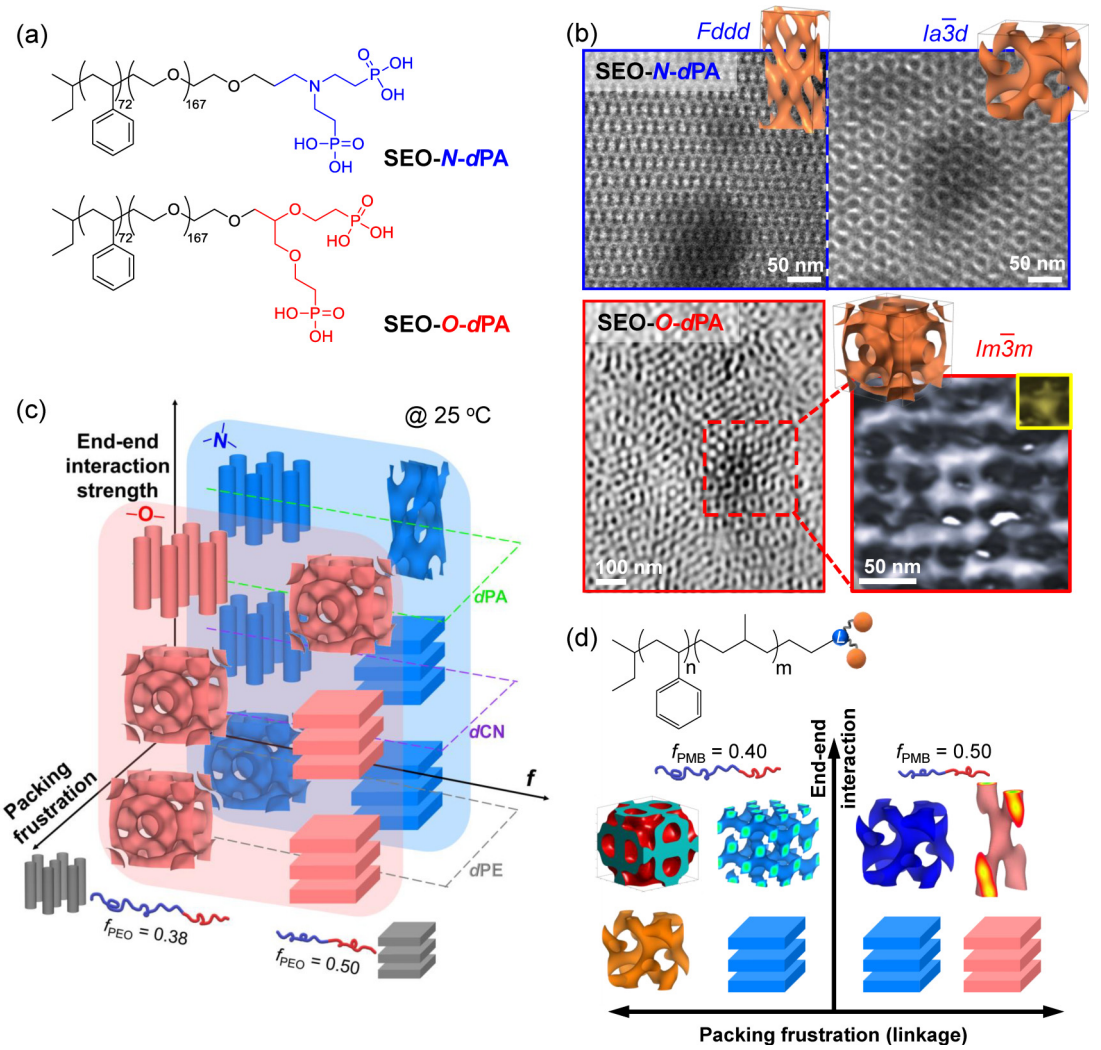

FIG. 14. (a) Chemical structures of PS-*b*-PEO having diphosphonic acid (*d*PA) end groups connected through different linkages. (b) TEM images and TEM tomography images of SEO-*N*-*d*PA and SEO-*O*-*d*PA. (c) Phase diagram of PS-*b*-PEOs having different types of di-end groups and linker molecules. The strength of end-end interaction and the degree of packing frustration were included as variables. (d) Chemical structure and phase diagram of di-end-functionalized PS-*b*-PMBs using different linker molecules. Reproduced from Ref. [98]. Copyright 2024 American Association for the Advancement of Science.

structures was observed [Fig. 14(b)], with *Fddd* being dominant. Notably, upon changing only one linker molecule from amine to ether, SEO-*O*-*d*PA exhibited a DP ($Im\bar{3}m$) structure, as visualized by tomography images and a captured TEM image in the bottom insets of Fig. 14(b).

The DP structure in SEO-*O*-*d*PA was confirmed to be in equilibrium state at room temperature by investigating morphological changes under different thermal histories. Upon heating, an order-order transition from DP to DG was observed, but upon cooling the sample back to room temperature, the DP structure reformed. This structure remained unchanged during a monitoring period of 22 months. This indicates that the packing frustration of network structures in SEO can be modulated by end groups and linker molecules, constituting less than 1% of the overall number of repeating units.

To control the strength of the end-end interactions, different di-end functional groups, including *d*CN (di-nitrile) and *d*PE (di-phosphoethoxy), were also introduced. The stability of hexapod intersections over tripod ones was determined by the interplay between the strength of the end-end interactions and the initial curvature shape. When the PEO content was minor and the end-end interaction was modest, diverse di-end-functionalized SEOs achieved an equilibrium Schwarz P surface [Fig. 14(c); ether and amine linkages are colored red and blue, respectively]. The enhanced end-end interactions within the minor PEO domains stabilized the curved curvatures to afford hex structures. In SEOs with symmetric compositions, the realization of a constant mean curvature of the P surface requires excessive chain stretching and high concentration fluctuations for the PEO chains to form a flat interface, a condition met only by SEO-*O*-*d*PA with strong end-end interactions. The occurrence of equilibrium DP structures in linear diblock copolymers represents a notable milestone.

To validate the versatility of employing end-group and linker chemistries for stabilizing complex 3D network structures in diblock copolymers, irrespective of the

chemical details of the polymer backbones, Park *et al.* synthesized additional sets of block copolymers, polystyrene-*b*-polymethylbutylene (PS-*b*-PMB), with varying block compositions. Figure 14(d) presents the phase diagram of di-end-functionalized PS-*b*-PMBs, delineated based on the strength of end-end interactions and degree of packing frustration (type of linkage). These findings strongly support the crucial role of end-group and linker chemistries in achieving diverse 3D networks, e.g., DG, DD, and A15-like single networks, in diblock copolymers.

VII. OUTLOOK AND CONCLUSIONS

The exploration of 3D nanostructures in block copolymers is a promising field of material science, inspiring the development of innovative strategies (such as block interface manipulation, PDI modification, and selective solvent usage) for addressing packing frustration and enhancing thermodynamic stability. The incorporation of charged units into block copolymers for electrostatic control provides valuable insights into the stabilization of low-symmetry 3D morphologies. With the advancements in synthetic techniques, the future holds considerable potential for diverse nanostructures with precisely controlled sizes and shapes, offering numerous applications in various fields. The recent discoveries of DP structures in linear diblock copolymers and intriguing phase transitions among complex network structures driven by end groups and linker chemistry have advanced this research area.

We advocate revising conventional block copolymer phase diagrams to consider end-end interactions and end-group arrangements. In instances where end-functionalized block copolymers exhibit strong end-end interactions, the lam structures are confined to a narrower phase diagram window. Conversely, a broader phase window enables the stabilization of diverse network structures such as gyroid, diamond, and primitive phases. The generation of such structures, even in simple linear diblock copolymers, helps to advance scientific knowledge. This versatile approach can reveal unprecedented network structures in various soft materials, thereby driving advancements in nanotechnology. Future research should deepen our understanding of the self-assembly behavior of end-functionalized block copolymers.

ACKNOWLEDGMENTS

This work was supported by National Research Foundation of Korea (NRF) grants funded by the Korea Government (Grants No. NRF-2022R1A2C3004667, No. NRF-2017R1A5A1015365, and No. NRF-2018M3D1A1058624). We also acknowledge financial support from Korea Toray Science Foundation.

[1] F. H. Schacher, P. A. Rupar, and I. Manners, Functional block copolymers: Nanostructured materials with emerging applications, Angew. Chem., Int. Ed. Engl. **51**, 7898 (2012).

[2] L. Martín-Moreno, F. J. García-Vidal, and A. M. Somoza, Self-assembled triply periodic minimal surfaces as molds for photonic band gap materials, Phys. Rev. Lett. **83**, 73 (1999).

[3] J. B. Pendry, A. J. Holden, W. J. Stewart, and I. Youngs, Extremely low frequency plasmons in metallic mesostructures, Phys. Rev. Lett. **76**, 4773 (1996).

[4] D. R. Smith, W. J. Padilla, D. C. Vier, S. C. Nemat-Nasser, and S. Schultz, Composite medium with simultaneously negative permeability and permittivity, Phys. Rev. Lett. **84**, 4184 (2000).

[5] F. S. Bates, M. A. Hillmyer, T. P. Lodge, C. M. Bates, K. T. Delaney, and G. H. Fredrickson, Multiblock polymers: Panacea or Pandora's box?, Science **336**, 434 (2012).

[6] C. Nowak and F. A. Escobedo, Optimizing the network topology of block copolymer liquid crystal elastomers for enhanced extensibility and toughness, Phys. Rev. Mater. **1**, 035601 (2017).

[7] R. P. Collanton and K. D. Dorfman, Interfacial geometry in particle-forming phases of diblock copolymers, Phys. Rev. Mater. **6**, 015602 (2022).

[8] F. S. Bates, Polymer-polymer phase behavior, Science **251**, 898 (1991).

[9] F. S. Bates and G. H. Fredrickson, Block copolymer thermodynamics: Theory and experiment, Annu. Rev. Phys. Chem. **41**, 525 (1990).

[10] E. Helfand, Block copolymer theory. III. Statistical mechanics of the microdomain structure, Macromolecules **8**, 552 (1975).

[11] E. Helfand, Block copolymers, polymer-polymer interfaces, and the theory of inhomogeneous polymers, Acc. Chem. Res. **8**, 295 (1975).

[12] L. Leibler, Theory of microphase separation in block copolymers, Macromolecules **13**, 1602 (1980).

[13] C. Sinturel, F. S. Bates, and M. A. Hillmyer, High χ-low N block polymers: How far can we go?. ACS Macro Lett. **4**, 1044 (2015).

[14] L. Kumar, S. Singh, A. Horechyy, A. Fery, and B. Nandan, Block copolymer template-directed catalytic systems: Recent progress and perspectives, Membranes **11**, 318 (2021).

[15] Y. C. Lu, P. C. Tseng, M. J. Yang, C. J. Wang, Y. C. Ling, C. F. Lin, and H. Y. Hsueh, Fabrication of gyroid-structured metal/semiconductor nanoscaffolds with ultrasensitive SERS detection via block copolymer templating, Adv. Opt. Mater. **11**, 2202280 (2023).

[16] H.-Y. Hsueh, Y.-C. Ling, H.-F. Wang, L.-Y. C. Chien, Y.-C. Hung, E. L. Thomas, and R. -M. Ho, Shifting networks to achieve subgroup symmetry properties, Adv. Mater. **26**, 3225 (2014).

[17] E.-L. Lin, W.-L. Hsu, and Y.-W. Chiang, Trapping structural coloration by a bioinspired gyroid microstructure in solid state, ACS Nano **12**, 485 (2018).

[18] R. Dehmel, A. Nicolas, M. R. J. Scherer, and U. Steiner, 3D nanostructured conjugated polymers for optical applications, Adv. Funct. Mater. **25**, 6900 (2015).

[19] Y. La, C. Park, T. J. Shin, S. H. Joo, S. Kang, and K. T. Kim, Colloidal inverse bicontinuous cubic membranes of block copolymers with tunable surface functional groups, Nat. Chem. **6**, 534 (2014).

[20] H. Sai, K. W. Tan, K. Hur, E. Asenath-Smith, R. Hovden, Y. Jiang, M. Riccio, D. A. Muller, V. Elser, L. A. Estroff, S. M. Gruner, and U. Wiesner, Hierarchical porous polymer scaffolds from block copolymers, Science **341**, 530 (2013).

[21] H.-Y. Hsueh, H.-Y. Chen, M.-S. She, C.-K. Chen, R.-M. Ho, S. Gwo, H. Hasegawa, and E. L. Thomas, Inorganic gyroid with exceptionally low refractive index from block copolymer templating, Nano Lett. **10**, 4994 (2010).

[22] K. Hur, Y. Francescato, V. Giannini, S. A. Maier, R. G. Hennig, and U. Wiesner, Three-dimensionally isotropic negative refractive index materials from block copolymer self-assembled chiral gyroid networks, Angew. Chem., Int. Ed. **50**, 11985 (2011).

[23] K. D. Dorfman, Frank–Kasper phases in block polymers, Macromolecules **54**, 10251 (2021).

[24] L. Yan, C. Rank, S. Mecking, and K. I. Winey, Gyroid and other ordered morphologies in single-ion conducting polymers and their impact on ion conductivity, J. Am. Chem. Soc. **142**, 857 (2020).

[25] S. Choudhury, M. Agrawal, P. Formanek, D. Jehnichen, D. Fischer, B. Krause, V. Albrecht, M. Stamm, and L. Ionov, Nanoporous cathodes for high-energy Li-S batteries from gyroid block copolymer templates, ACS Nano **9**, 6147 (2015).

[26] D. A. Hajduk, P. E. Harper, S. M. Gruner, C. C. Honeker, G. Kim, L. J. Fetters, and G. Kim, The gyroid: A new equilibrium morphology in weakly segregated diblock copolymers, Macromolecules **27**, 4063 (1994).

[27] E. W. Cochran, C. J. Garcia-Cervera, and G. H. Fredrickson, Stability of the gyroid phase in diblock copolymers at strong segregation, Macromolecules **39**, 2449 (2006).

[28] S. Cui, B. Zhang, L. Shen, F. S. Bates, and T. P. Lodge, Core–shell gyroid in ABC bottlebrush block terpolymers, J. Am. Chem. Soc. **144**, 21719 (2022).

[29] M. W. Matsen, Effect of architecture on the phase behavior of AB-type block copolymer melts, Macromolecules **45**, 2161 (2012).

[30] P. Padmanabhan, F. Martinez-Veracoechea, and F. A. Escobedo, Computation of free energies of cubic bicontinuous phases for blends of diblock copolymer and selective homopolymer, Macromolecules **49**, 5232 (2016).

[31] M. W. Matsen and M. Schick, Stable and unstable phases of a linear multiblock copolymer melt, Macromolecules **27**, 7157 (1994).

[32] Q. Du, Z. Wang, S. Zhou, J. Zhao, and V. Kumar, Searching for cluster Lego blocks for three-dimensional and two-dimensional assemblies, Phys. Rev. Mater. **5**, 066001 (2021).

[33] A. Travesset, Nanoparticle superlattices as quasi-Frank-Kasper phases, Phys. Rev. Lett. **119**, 115701 (2017).

[34] M. W. Matsen and F. S. Bates, Origins of complex self-assembly in block copolymers, Macromolecules **29**, 7641 (1996).

[35] A. J. Meuler, M. A. Hillmyer, and F. S. Bates, Ordered network mesostructures in block polymer materials, Macromolecules **42**, 7221 (2009).

[36] R. Roy, J. K. Park, W. S. Young, S. E. Mastroianni, M. S. Tureau, and T. H. Epps, Double-gyroid network morphology in tapered diblock copolymers, Macromolecules **44**, 3910 (2011).

[37] J. R. Brown, S. W. Sides, and L. M. Hall, Phase behavior of tapered diblock copolymers from self-consistent field theory, ACS Macro Lett. **2**, 1105 (2013).

[38] B. Yu, R. Li, and R. A. Segalman, Tuning the double gyroid phase window in block copolymers via polymer chain conformation near the interface, Macromolecules **54**, 5388 (2021).

[39] N. A. Lynd and M. A. Hillmyer, Influence of polydispersity on the self-assembly of diblock copolymers, Macromolecules **38**, 8803 (2005).

[40] N. A. Lynd, A. J. Meuler, and M. A. Hillmyer, Polydispersity and block copolymer self-assembly, Prog. Polym. Sci. **33**, 875 (2008).

[41] A. J. Meuler, C. J. Ellison, M. A. Hillmyer, and F. S. Bates, Polydispersity-induced stabilization of the core–shell gyroid, Macromolecules **41**, 6272 (2008).

[42] M. W. Matsen, Phase behavior of block copolymer/homopolymer blends, Macromolecules **28**, 5765 (1995).

[43] K. I. Winey, E. L. Thomas, and L. J. Fetters, The ordered bicontinuous double-diamond morphology in diblock copolymer/homopolymer blends, Macromolecules **25**, 422 (1992).

[44] F. J. Martinez-Veracoechea and F. A. Escobedo, Bicontinuous phases in diblock copolymer/homopolymer blends: Simulation and self-consistent field theory, Macromolecules **42**, 1775 (2009).

[45] T. H. Epps, E. W. Cochran, C. M. Hardy, T. S. Bailey, R. S. Waletzko, and F. S. Bates, Network phases in ABC triblock copolymers, Macromolecules **37**, 7085 (2004).

[46] Y. Masushita, J. Suzuki, and M. Seki, Surfaces of tricontinuous structure formed by an ABC triblock copolymer in bulk, Phys. B: Condens. Matter **248**, 238 (1998).

[47] T. A. Shefelbine, M. E. Vigild, M. W. Matsen, D. A. Hajduk, M. A. Hillmyer, E. L. Cussler, and F. S. Bates, Core−shell gyroid morphology in a poly(isoprene-block-styrene-block-dimethylsiloxane) triblock copolymer, J. Am. Chem. Soc. **121**, 8457 (1999).

[48] T. S. Bailey, C. M. Hardy, T. H. Epps, and F. S. Bates, A noncubic triply periodic network morphology in poly(isoprene-*b*-styrene-*b*-ethylene oxide) triblock copolymers, Macromolecules **35**, 7007 (2002).

[49] M. Takenaka, T. Wakada, S. Akasaka, S. Nishitsuji, K. Saijo, H. Shimizu, M. I. Kim, and H. Hasegawa, Orthorhombic *Fddd* network in diblock copolymer melts, Macromolecules **40**, 4399 (2007).

[50] S. Lee, M. J. Bluemle, and F. S. Bates, Discovery of a Frank-Kasper σ phase in sphere-forming block copolymer melts, Science **330**, 349 (2010).

[51] J. Zhang and F. S. Bates, Dodecagonal quasicrystalline morphology in a poly(styrene-*b*-isoprene-*b*-styrene-*b*-ethylene oxide) tetrablock terpolymer, J. Am. Chem. Soc. **134**, 7636 (2012).

[52] S. Chanpuriya, K. Kim, J. Zhang, S. Lee, A. Arora, K. D. Dorfman, K. T. Delaney, G. H. Fredrickson, and F. S. Bates, Cornucopia of nanoscale ordered phases in sphere-forming tetrablock terpolymers, ACS Nano **10**, 4961 (2016).

[53] S. T. Milner, Chain architecture and asymmetry in copolymer microphases, Macromolecules **27**, 2333 (1994).

[54] P. D. Olmsted and S. T. Milner, Strong segregation theory of bicontinuous phases in block copolymers, Macromolecules **31**, 4011 (1998).

[55] G. M. Grason, B. A. DiDonna, and R. D. Kamien, Geometric theory of diblock copolymer phases, Phys. Rev. Lett. **91**, 058304 (2003).

[56] G. M. Grason and R. D. Kamien, Interfaces in diblocks: A study of miktoarm star copolymers, Macromolecules **37**, 7371 (2004).
[57] N. Xie, W. Li, F. Qiu, and A.-C. Shi, σ Phase formed in conformationally asymmetric AB-type block copolymers, ACS Macro Lett. **3**, 906 (2014).
[58] Q. Dong and W. Li, Effect of molecular asymmetry on the formation of asymmetric nanostructures in ABC-type block copolymers, Macromolecules **54**, 203 (2021).
[59] Y. Seo, D. Woo, L. Li, W. Li, and J. K. Kim, Phase behavior of PS-(PS-*b*-P2VP)$_3$ miktoarm star copolymer, Macromolecules **54**, 7822 (2021).
[60] M. W. Matsen and F. S. Bates, Block copolymer microstructures in the intermediate-segregation regime, J. Chem. Phys. **106**, 2436 (1997).
[61] G. M. Grason and R. D. Kamien, Self-consistent field theory of multiply branched block copolymer melts, Phys. Rev. E **71**, 051801 (2005).
[62] M. Watanabe, Y. Asai, J. Suzuki, A. Takano, and Y. Matsushita, Frank-Kasper A15 phase formed in AB$_n$ block-graft copolymers with large numbers of graft chains, Macromolecules **53**, 10217 (2020).
[63] M. W. Bates, J. Lequieu, S. M. Barbon, R. M. Lewis, K. T. Delaney, A. Anastasaki, C. J. Hawker, G. H. Fredrickson, and C. M. Bates, Stability of the A15 phase in diblock copolymer melts, Proc. Natl. Acad. Sci. USA **116**, 13194 (2019).
[64] C. Y. Chu, W. F. Lin, J. C. Tsai, C. S. Lai, S. C. Lo, H. L. Chen, and T. Hashimoto, Order–order transition between equilibrium ordered bicontinuous nanostructures of double diamond and double gyroid in stereoregular block copolymer, Macromolecules **45**, 2471 (2012).
[65] C.-H. Lin, T. Higuchi, H.-L. Chen, J.-C. Tsai, H. Jinnai, and T. Hashimoto, Stabilizing the ordered bicontinuous double diamond structure of diblock copolymer by configurational regularity, Macromolecules **51**, 4049 (2018).
[66] C. Y. Chu, X. Jiang, H. Jinnai, R. Y. Pei, W. F. Lin, J. C. Tsai, and H. L. Chen, Real-space evidence of the equilibrium ordered bicontinuous double diamond structure of a diblock copolymer, Soft Matter **11**, 1871 (2015).
[67] M. W. Bates, S. M. Barbon, A. E. Levi, R. M. Lewis III, H. K. Beech, K. M. Vonk, C. Zhang, G. H. Fredrickson, C. J. Hawker, and C. M. Bates, Synthesis and self-assembly of AB$_n$ miktoarm star polymers, ACS Macro Lett. **9**, 396 (2020).
[68] M. J. Park and N. P. Balsara, Phase behavior of symmetric sulfonated block copolymers, Macromolecules **41**, 3678 (2008).
[69] C. E. Sing, J. W. Zwanikken, and M. Olvera de la Cruz, Electrostatic control of block copolymer morphology, Nat. Mater. **13**, 694 (2014).
[70] S. Y. Kim, S. Kim, and M. J. Park, Enhanced proton transport in nanostructured polymer electrolyte/ionic liquid membranes under water-free conditions, Nat. Commun. **1**, 88 (2010).
[71] O. Kim, K. Kim, U. H. Choi, and M. J. Park, Tuning anhydrous proton conduction in single-ion polymers by crystalline ion channels, Nat. Commun. **9**, 5029 (2018).
[72] O. Kim, S. Y. Kim, H. Ahn, C. W. Kim, Y. M. Rhee, and M. J. Park, Phase behavior and conductivity of sulfonated block copolymers containing heterocyclic diazole-based ionic liquids, Macromolecules **45**, 8702 (2012).
[73] O. Kim, S. Y. Kim, J. Lee, and M. J. Park, Building less tortuous ion-conduction pathways using block copolymer electrolytes with a well-defined cubic symmetry, Chem. Mater. **28**, 318 (2016).
[74] H. Y. Jung, O. Kim, and M. J. Park, Ion transport in nanostructured phosphonated block copolymers containing ionic liquids, Macromol. Rapid Commun. **37**, 1116 (2016).
[75] J. Min, H. Jung, S. Jung, B. Lee, C. Y. Son, and M. J. Park, Enhancing ion transport in charged block copolymers by stabilizing low symmetry morphology: Electrostatic control of interfaces, Proc. Natl. Acad. Sci. USA **118**, e2107987118 (2021).
[76] M. W. Matsen and F. S. Bates, Conformationally asymmetric block copolymers, J. Polym. Sci., Part B: Polym. Phys. **35**, 945 (1997).
[77] K. Kim, M. W. Schulze, A. Arora, R. M. Lewis, M. A. Hillmyer, K. D. Dorfman, and F. S. Bates, Thermal processing of diblock copolymer melts mimics metallurgy, Science **356**, 520 (2017).
[78] T.-Y. Lo, C.-C. Chao, R.-M. Ho, P. Georgopanos, A. Avgeropoulos, and E. L. Thomas, Phase transitions of polystyrene-*b*-poly(dimethylsiloxane) in solvents of varying selectivity, Macromolecules **46**, 7513 (2013).
[79] C. Y. Chang, G. M. Manesi, C. Y. Yang, Y. C. Hung, K. C. Yang, P. T. Chiu, A. Avgeropoulos, and R. M. Ho, Mesoscale networks and corresponding transitions from self-assembly of block copolymers, Proc. Natl. Acad. Sci. USA **118**, e2022275118 (2021).
[80] X. Zeng, G. Ungar, and M. Impéror-Clerc, A triple-network tricontinuous cubicliquid crystal, Nat. Mater. **4**, 562 (2005).
[81] Y. Cao, M. Alaasar, L. Zhang, C. Zhu, C. Tschierske, and F. Liu, Supramolecular meso-trick: Ambidextrous mirror symmetry breaking in a liquid crystalline network with tetragonal symmetry, J. Am. Chem. Soc. **144**, 6936 (2022).
[82] S. Poppe, C. Chen, F. Liu, and C. Tschierske, A skeletal double gyroid formed by single coaxial bundles of catechol based bolapolyphiles, Chem. Commun. **54**, 11196 (2018).
[83] X. Zeng, M. Prehm, G. Ungar, C. Tschierske, and F. Liu, Formation of a double diamond cubic phase by thermotropic liquid crystalline self-assembly of bundled bolaamphiphiles, Angew. Chem., Int. Ed. **55**, 8324 (2016).
[84] X. Zeng, S. Poppe, A. Lehmann, M. Prehm, C. Chen, F. Liu, H. Lu, G. Ungar, and C. Tschierske, A self-assembled bicontinuous cubic phase with a single-diamond network, Angew. Chem., Int. Ed. **58**, 7375 (2019).
[85] S. Poppe, X. Cheng, C. Chen, X. Zeng, R. B. Zhang, F. Liu, G. Ungar, and C. Tschierske, Liquid organic frameworks: The single-network "Plumber's Nightmare" bicontinuous cubic liquid crystal, J. Am. Chem. Soc. **142**, 3296 (2020).
[86] C. Tschierske, Development of structural complexity by liquid-crystal self-assembly, Angew. Chem., Int. Ed. **52**, 8828 (2013).
[87] Z. Su, C.-h. Hsu, Z. Gong, X. Feng, J. Huang, R. Zhang, Y. Wang, J. Mao, C. Wesdemiotis, T. Li, S. Seifert, W. Zhang, T. Aida, M. Huang, and S. Z. D. Cheng, Identification of a Frank-Kasper Z phase from shape amphiphile self-assembly, Nat. Chem. **11**, 899 (2019).
[88] K. Yue, M. Huang, R. L. Marson, J. He, J. Huang, Z. Zhou, J. Wang, C. Liu, X. Yan, K. Wu, Z. Guo, H. Liu, W. Zhang, P. Ni, C. Wesdemiotis, W.-B. Zhang, S. C. Glotzer, and S. Z. D. Cheng, Geometry induced sequence of nanoscale Frank–Kasper and quasicrystal mesophases in giant surfactants, Proc. Natl. Acad. Sci. USA **113**, 14195 (2016).

[89] J. Huang, Z. Su, M. Huang, R. Zhang, J. Wang, X. Feng, R. Zhang, W. Shan, X.-Y. Yan, Q.-Y. Guo, T. Liu, Y. Liu, Y. Cui, X. Li, A.-C. Shi, and S. Z. D. Cheng, Spherical supramolecular structures constructed via chemically symmetric perylene bisimides: Beyond columnar assembly, Angew. Chem., Int. Ed. **59**, 18563 (2020).

[90] F. Ishiwari, G. Okabe, H. Ogiwara, T. Kajitani, M. Tokita, M. Takata, and T. Fukushima, Terminal functionalization with a triptycene motif that dramatically changes the structural and physical properties of an amorphous polymer, J. Am. Chem. Soc. **140**, 13497 (2018).

[91] V. Schädler, J. Spickermann, H. J. Räder, and U. Wiesner, Synthesis and characterization of α,ω-macrozwitterionic block copolymers of styrene and isoprene, Macromolecules **29**, 4865 (1996).

[92] V. Schädler and U. Wiesner, Salt-controlled lamellar spacing in ionically end-capped symmetric diblock copolymers, Macromolecules **30**, 6698 (1997).

[93] G. Jo, H. Ahn, and M. J. Park, Simple route for tuning the morphology and conductivity of polymer electrolytes: One end functional group is enough, ACS Macro Lett. **2**, 990 (2013).

[94] H. Y. Jung, P. Mandal, G. Jo, O. Kim, M. Kim, K. Kwak, and M. J. Park, Modulating ion transport and self-assembly of polymer electrolytes via end-group chemistry, Macromolecules **50**, 3224 (2017).

[95] A. Reddy, M. S. Dimitriyev, and G. M. Grason, Medial packing and elastic asymmetry stabilize the double-gyroid in block copolymers, Nat. Commun. **13**, 2629 (2022).

[96] M. S. Dimitriyev, A. Reddy, and G. M. Grason, Medial packing, frustration, and competing network phases in strongly segregated block copolymers, Macromolecules **56**, 7184 (2023).

[97] A. Reddy, X. Feng, E. L. Thomas, and G. M. Grason, Block copolymers beneath the surface: Measuring and modeling complex morphology at the subdomain scale, Macromolecules **54**, 9223 (2021).

[98] H. Lee, S. Kwon, J. Min, S.-M. Jin, J. H. Hwang, E. Lee, W. B. Lee, and M. J. Park, Thermodynamically stable plumber's nightmare structures in block copolymers, Science **383**, 70 (2024).